UNIVERSITY OF WISCONSIN
Cardiovascular Research Center

Cardiovascular Research Summit & Poster Fair

Therapeutic Strategies For Cardiovascular Disease

October 12, 2023

Wisconsin Institute for Discovery
330 N. Orchard St.
Madison, WI

School of Medicine and Public Health
UNIVERSITY OF WISCONSIN–MADISON

CARDIOVASCULAR RESEARCH CENTER
Annual Scientific Poster Fair
Thursday, October 12, 2023

POSTER SUMMARY

Poster No.	Last Name	First Name	Department Affiliation	PI / Lab	Title
Undergraduate					
1	**Hoth**	**Annabelle**	Neuroscience	Robertson	hERG1a/1b mRNAs Interact to Promote Ion Channel Biogenesis
2	**Jang**	**Jay**	Medicine	Kamp	Utilization of Poly(I:C) with Subsequent T3 Treatment for Maturation of Induced Pluripotent Stem Cell-Derived Cardiomyocytes
3	**Kaska**	**Sara**	Medicine	Eckhardt	Functional Characterization of Ca^{2+} Handling in Andersen-Tawil Syndrome Causing G300D-*KCNJ2* Mice
4	**Milaitis**	**Maxwell**	Medicine	Eckhardt	Micropatterned Culture Substrate for hiPSC Modeling of Idiopathic Ventricular Fibrillation
5	**Sabel**	**Anna**	Cell & Regenerative Biology	Lo Sardo	The Role of ANRIL lncRNA in Vascular Smooth Muscle Cells
Graduate					
6	**Stroik**	**Dawson**	Pathology and Laboratory Medicine	Guo	Altering Titin Size Through Antisense Oligonucleotides to Treat HFpEF
7	**Aballo**	**Timothy**	Cell & Regenerative Biology	Ge	Transgenic Expression of Slow Skeletal Troponin I Promotes Cardiac Regeneration after Myocardial Infarction in Mice
8	**Begeman**	**Ian**	Cell & Regenerative Biology	Kang	Identifying Novel Cardiac Regeneration Enhancers by Utilizing Computational Analyses and Transgenic Assays
9	**de Medeiros Vieira**	**Carolina**	Cell & Regenerative Biology	Lo Sardo	Molecular Insights into the 9p21.3 CAD Risk Locus in Diverse Populations
10	**Dou**	**Yimeng**	Medical Physics	Varghese	Efficient Sensorless End-to-End Freehand Ultrasound with Physical Inspired Network
11	**Haley**	**Travis**	Kinesiology	Schrage	Cerebral blood flow responses to hyperoxia: exploring sex differences
12	**Josvai**	**Mitchell**	Biomedical Engineering	Crone	Altered Contractile Kinetics in a hiPSC-derived Cardiomyocyte Model of Hypertrophic Cardiomyopathy
13	**Kannan**	**Sudharsan**	Neuroscience	Robertson	A Novel ER Compartment as a Substrate for Heteromeric Ion Channel Assembly

Poster No.	Last Name	First Name	Department Affiliation	PI / Lab	Title
14	**Kim**	**Jooyong**	Cell & Regenerative Biology	Liu	lncRNA Zeb2os Regulates Macrophage Differentiation and Proliferation in Abdominal Aortic Aneurysm
15	**Kozitza**	**Callyn**	Biomedical Engineering	Witzenburg	A Computational Model of Pulmonary Artery Stenosis
16	**Nuttall**	**Dakota**	Cell & Regenerative Biology	Mahmoud	Elucidating the Transcriptional and Epigenetic Impact of Succinate Dehydrogenase Inhibition on Cardiac Regeneration
17	**Paltzer**	**Wyatt**	Cell & Regenerative Biology	Mahmoud	Elucidating the Role of Mechanistic Target of Rapamycin Complex 1 During Heart Regeneration
18	**Rice**	**James**	Mechanical Engineering	Roldan-Alzate	Hemodynamics in Coarctation of the Aorta using 4D Flow MRI, Computational Fluid Dynamics, and Particle Image Velocimetry
19	**Rogers**	**Holden**	Chemistry	Ge	Comprehensive Characterization of Endogenous Phospholamban Enabled by Top-Down Proteomics and Photocleavable Surfactant
20	**Rossler**	**Kalina**	Cell & Regenerative Biology	Ge	Integrated Proteomics Analysis of *In Vitro* Hypertrophic Cardiomyopathy Models
21	**Salido**	**Elsa**	Cell & Regenerative Biology	Lo Sardo	9p21.3 Coronary Artery Disease Risk Locus and Vascular Function
22	**Song**	**Ruolin**	Comparative Biosciences	Kumar	Gestational Intermittent Hypoxia-Induced Endothelial Dysfunction and Hypertension in Pregnant Rats: Evidence for a Role of Endothelin Type B Receptor
23	**Suryavanshi**	**Shraddha**	Cell & Regenerative Biology	Lo Sardo	9p21.3 CAD Risk Locus and mRNA Regulation
24	**Turner**	**Daniel**	Medicine	Glukhov	Neutral Sphingomyelinase Mediates Phenotypes of Cardiac Hypertrophy
25	**Vidya Dangudubiyyam**	**Sri**	Comparative Biosciences	Kumar	Angiotensin Type 2 Receptor Activation Reverses PFOS-Induced Uterine Vascular Hyper-Reactivity and Hypertension in Pregnancy
26	**Wagner**	**Matthew**	Cell & Regenerative Biology	Blum	Roundabout Receptors are Required for Maintaining Islet Architecture during Acute Pancreatitis
27	**Wancewicz**	**Benjamin**	Cell & Regenerative Biology	Ge	Evaluation of Multiple Extraction Methods for the Analysis of Human Heart Metabolites

Poster No.	Last Name	First Name	Department Affiliation	PI / Lab	Title
28	**Xioa**	**Li**	Medicine	Valdivia	Structure-Function Analysis of Two Novel Calcins Based on a Transcriptomic Comparison of East Asian Scorpions
29	**Yang**	**Qianfan**	Cell & Regenerative Biology	Liu	Extracellular Vesicles and Abdominal Aortic Aneurysm
30	**Zade**	**Rohan**	Cell & Regenerative Biology	Lo Sardo	The 9p21 Risk Locus Controls Cell Motility in Vascular Smooth Muscle Cells
	Postdoctoral, Scientists & Faculty				
31	**Bontekoe**	**Jack**	Surgery	Liu	Upregulation Of Receptor Interacting Protein Kinase-3 Augments Abdominal Aortic Aneurysms
32	**de Lange**	**Willem**	Pediatrics	Ralphe	Chronic Mavacamten Treatment Has Opposing Effects on Contractility in Engineered Heart Tissue Models of Severe vs. Mild Hypertrophic Cardiomyopathy
33	**Gober**	**Leah**	Surgery	Roldan-Alzate	Noninvasive Assessment of Mechanical Properties using 4D flow MRI in a Porcine Model of Aortic Coarctation
34	**Gregorich**	**Zachery**	Animal & Dairy Sciences	Guo	Sequestration of Alternative Splicing Factors in Cytoplasmic RBM20 Granule Contributes to Aberrant Splicing in RBM20 Cardiomyopathy
35	**Krichel**	**Boris**	Cell & Regenerative Biology	Ge	A Bioanalytical Perspective on AMPK Activation: Phosphorylation, Small Molecule Binding and Isoform Specific Allostery Analyzed with Native and Top-Down MS
36	**Medvedev**	**Roman**	Medicine	Glukhov	Sphingomyelinase-Induced ROS Production Suppresses Cardiac Performance
37	**Mertens**	**Jasmine**	Pediatrics	Ralphe	A Missense W792R Mutation in C6 Domain of Cardiac Myosin Binding Protein-C Alters Morphology and Contractility in Neonatal Mouse Myocardium
38	**Munawar**	**Saba**	Medicine	Eckhardt	Functional Impact of Phosphorylation-Site Mutations on PKA Response of Kir2.1
39	**Pergande**	**Melissa**	Cell & Regenerative Biology	Ge	Identification of Molecular Signatures of Ischemic Cardiomyopathy using Mass Spectrometry
40	**Ponce-Balbuena**	**Daniela**	Medicine	Valdivia	Cardiac $Na_V1.5$ Channel Exhibits a p38MAPK-Dependent Modulation
41	**Reilly**	**Louise**	Medicine	CMARP	Determining Underlying Mechanisms of Idiopathic VF: A Multi-Disciplinary Approach

Poster No.	Last Name	First Name	Department Affiliation	PI / Lab	Title
42	**Siri-Angkul**	**Natthaphat**	Medicine	Kamp	Leucine-Rich Repeat-Containing Protein 10 Potentiates L-Type Calcium Current Through Short-N-Terminus and Long-N-Terminus Isoforms of $Ca_V1.2$
43	**Voelker**	**Taylor**	Neuroscience	Robertson	Chronic Angiotensin II Signaling Triggers Sustained PIP_2 Deficits and Altered Sarcolemmal CaV1.2 Expression and Function in Cardiomyocytes
44	**Wolff**	**Matthew**	Medicine	Wolff	Effect of mTOR Inhibition on Left Ventricular Function in a Model of LMNA-associated Familial Dilated Cardiomyopathy
45	**Zheng**	**Jingjing**	Medicine	Alvarado	Mice with Three Major Phosphorylation Sites Ablation on RyR2 Have Normal Adrenergic Response but Increased Susceptibility to Ventricular Arrhythmia
46	**Zhou**	**Ting**	Cell & Regenerative Biology	Liu	Intricate Roles of Myeloid-derived Thrombospondin-1 in Aortic Aneurysm and Rupture

hERG1a/1b mRNAs Interact to Promote Ion Channel Biogenesis

Annabelle Hoth, Lisandra Flores-Aldama, Gail Robertson
Department of Neuroscience, School of Medicine and Public Health,
University of Wisconsin-Madison, Madison, WI, 53705

Background:
The *human ether-à-go-go-related gene* (*hERG*) encodes the voltage-gated potassium channel Kv11.1, also known as the hERG1 channel. This channel elicits the delayed rectifier potassium current, I_{Kr}, which is critical for repolarizing the ventricular action potential (Sanguinetti & Jurkiewicz, 1990). Inherited mutations affecting the function or expression of hERG1 channels have been related to the reduction of I_{Kr} currents and consequent prolongation of the duration of the ventricular action potential in cardiomyocytes (Sanguinetti et al., 1995; Trudeau et al., 1995). Therefore, the mechanisms underlying hERG1 function and expression have been widely studied (Vandenberg et al., 2012; Robertson & Morais-Cabral, 2020). In cardiomyocytes, functional hERG1 channels are heterotetramers of hERG1a and 1b subunits (Morias-Cabral JH, et al., 1998), which are encoded by alternate transcripts of the *hERG* gene and differ in their N-termini. hERG1a has a longer N-terminus containing the Per-Arnt-Sim (PAS)-cap, PAS, and N-linker domains, whereas 1b has a unique and short N-terminus region (Morias- Cabral JH, et al., 1998). hERG1a/1b heteromerization is vital for normal cardiomyocyte functioning, as an imbalance of these subunits' expression leads to pro-arrhythmic cellular behaviors (Jones et al., 2014; Feng et al., 2021). Our lab has shown that the N-termini of hERG1a and 1b subunits interact to form heteromeric channels (Phartiyal et al., 2007), and this oligomerization is facilitated by the co-translational association of the encoding mRNAs (Liu et al., 2016). Nevertheless, many details about the cotranslational process remain unknown. I propose that *hERG1a* and *1b* mRNAs directly interact *in vitro* in a structure-dependent manner.

Methods:
hERG1a and 1b plasmids were linearized with the EcoRI-HF enzyme (Biolabs) and then used for mRNA *in vitro* transcription (T7 mMessage mMachine, Invitrogen). After checking their structural integrity on an agarose gel, *in vitro* transcribed mRNAs were labeled (Label IT, Mirus). Wildtype and mutant *1a* mRNAs were labeled with Cy3 fluorescent dyes, while *1b* was labeled with Cy5. These mRNAs were then used for *in vitro* or HeLa live cell imaging. To evaluate the relevance of the mRNA secondary structure in the assembly of the co-translational complex, I compared the morphology and colocalization of the formed complexes between differently structured mRNA. Differences in the formation of complexes were used as a proxy for changes in the mRNA interactions.

Results:
We found that *hERG1a* and *1b* mRNAs form microscopic complexes and interact *in vitro.* This association was affected by *hERG1a* structure as we observed smaller complexes when co-incubating *hERG1b* with mutant hERG1a mRNAs. *hERG1a/1b* mRNA association was also observed in HeLa, after the co-transfection of the mRNAs, suggesting that co-transcription is not required for the association. These results suggest that the structural properties of the mRNA modulate their association and specificity of the process in cells.

Discussion:
This project will be the first to describe the relevance of mRNA structure on the biogenesis of heteromeric hERG1 channels and opens avenues to study the role of synonymous LQTS-related mutations, which alter only the mRNA sequence but not its encoded protein. Once completed, this work will be prepared for publication and will contribute novel insights into the mechanisms of LQTS and sudden cardiac death.

Utilization of Poly(I:C) with Subsequent T3 Treatment for Maturation of Induced Pluripotent Stem Cell-Derived Cardiomyocytes

Jay Jang[1], Natthaphat Siri-Angkul[1], Vladislav Leonov[1], Timothy J. Kamp[1]
[1]Department of Medicine, Cell and Regenerative Biology

Background: Therapeutic, research, and drug development uses of induced pluripotent stem cell-derived cardiomyocytes (iPSC-CM) are limited due to their immature nature. While progress has been made in advancing their maturation, replicating the phenotype of a native adult heart remains challenging. Polyinosinic:polycytidylic acid (pIC), a double-stranded RNA and a TLR3 ligand, activates NF-κB. Research indicates pIC might accelerate iPSC-CM maturation, notably through epigenetic changes like deactivation of type 2 Histone deacetylases (HDAC). Given that triiodothyronine (T3) plays a pivotal role in rapid post-natal cardiac development – by binding with nuclear thyroid hormone receptors which then interact with DNA to regulate gene expressions linked to cardiac maturation – I hypothesize that the induction of pIC during the progenitor stage of iPSC-CMs increase accessibility of the DNA and acts as a permissive factor for T3-mediated maturation.

Methods: iPSC-CMs were differentiated using the GiWi protocol. pIC (95ug/cm^2) treatment was administered from the 3rd to 5th day of differentiation, followed by T3 treatment (100nM) ± dexamethasone (100ng/mL) from day 17 to 25. Cells were harvested on day 25, analyzed on day 30, and maturation was characterized via qPCR for expression of genes associated with maturation (*KCNJ2, GJA1, TNNI3, and MYL2)*, optical mapping of monolayers on glass coverslips coated with Corning Synthemax, and patch clamping for action potentials and L-type Ca^{2+} currents.

Results: Relative to control, all four treatment groups (pIC+T3, T3, Dex+T3, and pIC) in a single experiment showed an increase in the expression of *KCNJ2*, *TNNI3*, and *MYL2*. Dex+T3 induced the highest level of *TNNI3* and *MYL2* while pIC+T3 showed the lowest increase. Transmembrane voltage measurements, using optical mapping, showed that control and all 4 test conditions generated comparable action potential durations and similar conduction velocities. Single-cell action potentials measured using the patch clamp isolated from control, pIC treated, and pIC+T3 treated iPSC-CMs demonstrated significant variability within groups with resting membrane potentials ranging from -40mV to -78mV and dV/dt_{max} being variable ranging from 20V/s to 230V/s. There were no significant differences in the action potential parameters across groups. Patch clamps studies showed that $I_{Ca,L}$ was of comparable magnitude in control and pIC+T3 groups.

Discussion: Our preliminary data show that all four tested strategies can increase gene expression of maturation markers in iPSC-CMs. Contrary to our hypothesis, pIC+T3 showed the least impact, while the T3+Dex group showed the greatest increase in maturation gene expression. Functional measures using optical mapping of monolayer action potentials, single cell action potentials, and $I_{Ca,L}$ show no clear differences between the groups tested. In the future, additional experiments are necessary to confirm the preliminary findings with improved procedures to enhance reproducibility. Furthermore, the disparity between gene expression findings and functional data will be addressed by matching the culture conditions exactly.

Functional Characterization of Ca^{2+} Handling in Andersen-Tawil Syndrome Causing G300D-*KCNJ2* Mice

Sara Kaska[1] , Saba Munawar[1], Corey Anderson[1], Louise Reilly[1], and Lee Eckhardt[1]
[1] *University of Wisconsin Madison Cellular and Molecular Arrhythmia Research Program*

Background

Andersen-Tawil syndrome (ATS) is a genetic disorder characterized by a phenotypic triad consisting of periodic paralysis, developmental dysmorphisms, and cardiac arrhythmias. The developmental dysmorphisms include micrognathia, low set ears, wide spaced eyes, syndactyly, and scoliosis. The ECG features include prolonged QTU and the arrhythmias observed are frequent premature ventricular contractions (PVCs), bidirectional ventricular tachycardia (BiVT), and polymorphic ventricular tachycardia (PMVT)[1]. Loss of function gene mutations in *KCNJ2* cause ATS and are autosomal dominant. *KCNJ2* encodes for Kir2.1, an inward rectifier potassium channel found in excitable cells, including neurons, skeletal muscle, smooth muscle, and cardiomyocytes. Bidirectional VT has been associated with overloaded intracellular Ca^{2+}calcium mishandling, yet the mechanistic link for BiVT in ATS has not been established. We hypothesize that dysfunctional Kir2.1 channels will lead to Ca^{2+} mishandling due to prolonged repolarization. Here, we study the G300D-*KCNJ2* mutation that has no functional current when expressed alone.

Methods

Genetically engineered mice were previously created to be heterozygous for G300D-*KCNJ2* ($G300D^{-/+}$) mutation. Ca^{2+} transients were measured using the IonOptix Calcium and Contractility System equipped with a Hyperswitch and MyoCam-S (IonOptix, Westwood, MA, USA) in isolated cardiomyocytes from $G300D^{-/+}$ vs. wild-type (WT) littermate controls. Cells were paced at 2-6Hz for 1 minute followed by 1 minute of rest. Isoproterenol (ISO, 10nM) was applied and the pacing protocol repeated. In a separate set of experiments, calcium tolerant ventricular myocytes were paced for 30 s at 2 Hz then treated with caffeine (10 mM). Experiments were conducted in a blinded fashion and revealed during data analysis.

Results

At baseline, WT myocytes have comparable basal Ca^{2+} between pacing frequencies. Additionally, peak CaT amplitude was similar between 2Hz and 4Hz at baseline and after ISO. Decay to 90% was comparable at baseline, however it was shortened at 2Hz following ISO. Tau was comparable between 2Hz and 4Hz at baseline and after ISO.

Discussion

The IonOptix system can be used to characterize Ca^{2+} transients in G300D-*KCNJ2* mice. An increase in intracellular Ca^{2+} has been linked to bidirectional VT, but the correlation with ATS is not clear.

1. Donaldson MR, Yoon G, Fu YH, Ptacek LJ. Andersen-Tawil syndrome: a model of clinical variability, pleiotropy, and genetic heterogeneity. Ann Med. 2004;36 Suppl 1:92-7. doi: 10.1080/17431380410032490. PMID: 15176430.

Micropatterned Culture Substrate for hiPSC Modeling of Idiopathic Ventricular Fibrillation

Maxwell Milaitis[1], Mitchell Josvai[2], Janay K Walters[1], Corey L. Anderson[1], Wendy C. Crone[2], Lee L. Eckhardt[1]
[1]University of Wisconsin Madison Cellular and Molecular Arrhythmia Research Program
[2]Department of Biomedical Engineering, University of Wisconsin-Madison, Madison, WI, USA

Background: Idiopathic Ventricular Fibrillation (IVF) causes sudden cardiac arrest/death (SCD) due to ventricular fibrillation but lacks monogenetic causes or structural biomarkers, making animal models untenable. We are using IVF patient-derived induced pluripotent stem cell-derived cardiomyocytes (iPSC-CMs) as a model for IVF. However, iPSC-CMs are hindered by morphological, mechanical, and electrophysiological immaturity. This work aims to help resolve these limitations by using previously reported micropatterning technology and co-culture of iPSC-CMs and cardiac fibroblasts (iPSC-CF) to better mimic the physiologic environment of the heart. We seek to utilize this system to characterize several IVF patient-derived iPSC-CMs in comparison to a control line.

Methods: IVF patient blood samples were reprogrammed into iPSCs by the Stem Cell Core at the Waisman Center. Due to the lack of disease-causing markers, familial controls may be inaccurate, we use a NIH registered non-diseased iPSC line for control. Patient and control iPSCs were then differentiated into iPSC-CMs and iPSC-CFs using standard protocols. Following differentiation, iPSC-CMs were affinity purified using magnetic-activated cell isolation and seeded on 10 kPa polydimethylsiloxane (PDMS) substrates with micropatterned Matrigel. After 4 days of micropatterned culture, patient-derived or control iPSC-CFs were seeded on the patterned substrates. The platform allows for an array of readouts to characterize patient CMs, including strain quantification, electrophysiological optical mapping, and immunocytochemistry.

Results: A pilot study was performed to optimize the differentiation and preparation of IVF iPSC-CMs. Day 30 IVF iPSC-CMs cultured on micropatterned substrates with iPSC-CFs were immunolabeled for DAPI, α-actinin, and N-Cadherin and compared to CMs cultured in a monolayer. N-cadherin staining was observed unstructured around CMs when grown as a monolayer. In contrast, N-cadherin appropriately localizes towards the ends of the cell-cell connections in the micropatterned plating, suggesting the formation of normal intercalated discs. Additionally, a-actinin staining in a monolayer showed poor sarcomere alignment and myofibrillar disarray, while cells grown on patterned substrates demonstrate well aligned sarcomeres. These results indicate that we have replicated a culture system that allows for more physiologically relevant morphological and structural iPSC-CM characteristics than monolayer culture systems.

Discussion: These results demonstrate a functional micropatterned culture system capable of supporting IVF patient-derived CM-CF coculture and several structural readouts. In the future, we seek to utilize optical mapping to characterize the electrophysiological properties of patient CMs in comparison to male and female control CMs. We also seek to use optical techniques to quantify the contractile properties of patient's and control CMs. These techniques will be used with the structural and morphological readouts we have previously demonstrated to characterize the phenotype of IVF patient CMs. These *in vitro* data will characterize the cellular phenotypic properties of the disorder to identify mechanistic-based anti-arrhythmic drug targets.

The Role of ANRIL lncRNA in Vascular Smooth Muscle Cells

Anna Sabel, Carolina de Medeiros Vieira, Rohan Zade, Valentina Lo Sardo
Department of Cell and Regenerative Biology, UW-Madison SMPH

Background:

Coronary artery disease (CAD) is a leading cause of death worldwide. CAD is caused by plaque buildup in the wall of arteries, often leading to myocardial infarction. The most influential genetic risk factor of CAD is the 9p21.3 locus. Within this locus, the CAD risk region is 60kb containing ~100 SNPs inherited together in the form of risk or non-risk. This locus is present only in humans and is a gene dessert, lacking coding genes. It does, however, overlap a long noncoding RNA (lncRNA), called ANRIL. Induced Pluripotent Stem Cell-derived Vascular Smooth Muscle Cells (iPSC-VSMCs) from individuals carrying the risk haplotype at 9p21.3 show increased ANRIL expression, compared to non-risk. Previous work in our lab found that ANRIL is not expressed in iPSCs and its expression increases over time throughout the VSMC differentiation, suggesting that ANRIL has a cell type-specific function. ANRIL is extensively spliced and it has been described in about 14 different linear isoforms. We previously showed that only four of these are expressed in VSMCs. Risk VSMCs show upregulation of ANRIL concomitant with a variety of functional defects and gene expression alterations. Modulation of ANRIL expression represents an exciting avenue to determine the role of this lncRNA in mediating normal VSMCs function and its role in genetic predisposition to CAD.

Methods

- Design and generate a CRISPRi lentiviral system for downregulation of ANRIL
- Test the efficacy of lentiviral particles in HEK cells
- Perform iPSC differentiation into VSMCs and optimize ANRIL knock down over time
- Expression analysis of risk-specific genes upon ANRIL knock down

Results

We successfully designed and cloned 4 different gRNAs for the downregulation of ANRIL. These gRNAs were combined with a CRISPRi system including a dCas9-KRAB construct. We generated lentiviral particles and tested different amounts on HEK cells, to determine the optimal concentration. We performed two independent iPSC to VSMC differentiation experiments to test the optimal time window to perform the ANRIL knockdown. Through testing different conditions, we were able to finalize the most effective gRNAs resulting in >60% knockdown of ANRIL in VSMCs. Moreover, we were able to identify the best time point during the VSMC differentiation to achieve successful knockdown. Finally, through gene expression profile we found that ANRIL silencing is sufficient to modulate the expression of genes exclusively expressed in risk VSMCs.

Discussion

The goal of this project was to develop a strategy to perform ANRIL knockdown in iPSC-derived VSMCs. We have successfully generated and tested a CRISPRi system to downregulate ANRIL to be used for future studies on VSMCs and other cell types. We have selected two optimal gRNAs and ruled out the best timing and condition to achieve successful knockdown. From our preliminary data, we have gained insight on the role of ANRIL in
controlling gene expression in VSMCs and we will continue to explore ANRIL target genes using this new tools.

Altering Titin Size Through Antisense Oligonucleotides to Treat HFpEF

Dawson Stroik[1, 2], Yanghai Zhang[2], Zachery R. Gregorich[2], Feng Jiang[3], Peng Yao[3], Wei Guo[1, 2]
[1]*Department of Pathology and Laboratory Medicine*
[2]*Department of Animal & Dairy Sciences*
[3]*University of Rochester School of Medicine and Dentistry*

Background:

Heart failure with preserved ejection fraction (HFpEF) is a heart disease that affects over 3 million people in the US alone and lacks effective treatments. HFpEF is characterized by diastolic dysfunction resulting from stiffening of the myocardium. The giant sarcomeric protein titin modulates the passive stiffness of the myocardium through post-translational modifications and isoform switching. Two classes of titin isoforms are expressed in the heart: longer and more compliant N2BA isoforms and a shorter and stiffer N2B isoform. The splicing factor RNA binding motif protein 20 (RBM20) binds the titin pre-mRNA and mediates exon exclusion resulting in expression of the shorter N2B isoform. Increased expression of larger N2BA isoforms has been shown to reduce myocardial stiffness and improve diastolic function. Thus, there is an interest in developing therapies targeting titin isoform switching to improve diastolic function in patients with HFpEF. However, promoting titin isoform switching via modulation of RBM20 expression is not ideal as disrupted splicing of RBM20 target genes results in systolic dysfunction and arrhythmia. Here, we designed antisense oligonucleotides (ASOs) targeting the RBM20 binding sites on the titin pre-mRNA in the hopes of promoting titin isoform switching without affecting the splicing of other target genes.

Methods:

We designed a titin-minigene comprised of alternatively spliced exons regulated by RBM20 and essential intron sequences. In silico analysis identified six potential RBM20 binding sites on the titin pre-mRNA and ASOs against these sites were designed. To test whether these ASOs promote titin isoform switching, we co-transfected the titin minigene construct with RBM20 or control plasmid (EGFP) to HEK293A cells. Co-transfected cells were treated with ASOs individually at concentrations of 10, 50, 100, or 200 nM for 48 hr. Altered splicing of the titin minigene was assessed by RT-PCR.

Results

Our results showed that one of the six ASOs (ASO-6) significantly ($p=0.0197$) disrupted RBM20-mediated exon exclusion at a dose of 100 nM. Without ASO treatment, cells expressed titin N2BA isoform about 19.9% of the total titin compared to 42.4% with ASO-6 treatment. There was an increase in N2BA isoform expression over N2B in cells treated with ASO-6 regardless of concentration, just not at significant levels until 100nM. Other ASO treatments lead to increased (ASO-1 and 3) or decreased (ASO-4) N2BA isoform expression but did not reach significance. Treatment with ASO-2 and 5 did not significantly impact RBM20-mediated splicing at any dose.

Conclusion:

This study demonstrated that targeting titin through ASO to change titin size could be a therapeutic strategy to reduce stiffness of the heart in human patients with HFpEF. Moving forward, we will test ASO-6 treatment in human cardiomyocytes and animal models with HFpEF.

Transgenic Expression of Slow Skeletal Troponin I Promotes Cardiac Regeneration after Myocardial Infarction in Mice

Timothy J. Aballo[1], Jiyoung Bae[2], Wyatt G. Paltzer[1], Emily A. Chapman[3], Rebecca Salamon[1], Morgan M. Mann[1], Ying Ge[1,3], Ahmed I. Mahmoud[1]

[1]*Department of Cell and Regenerative Biology, University of Wisconsin-Madison, Madison, WI*
[2]*Department of Nutritional Sciences, Oklahoma State University, Stillwater, OK*
[3]*Department of Chemistry, University of Wisconsin-Madison, Madison, WI*

Background: Heart failure (HF) is a leading cause of death worldwide, and despite its prevalence, there are no curative therapies. Adult mammalian cardiomyocytes (CMs) have very limited proliferative potential, and after myocardial infarction (MI), injured cardiac tissue is replaced with fibrotic scar rather than with functioning myocardium. Fascinatingly, the neonatal mouse heart possesses a regenerative capacity governed by CM proliferation; however, this regenerative capacity is lost by postnatal day 7 (P7). Interestingly, at P7, cardiac troponin I (cTnI, Tnni3) becomes the predominantly expressed troponin I (TnI) isoform, replacing slow skeletal troponin I (ssTnI, Tnni1). We hypothesize that expression of this key fetal sarcomeric protein (ssTnI) will promote cardiac regeneration in mice through increased CM proliferation.

Methods: Herein we utilize a transgenic (Tg) mouse line expressing ssTnI on the alpha-myosin heavy chain (α-MHC) promoter to explore the role of ssTnI during endogenous cardiac regeneration. Using global bottom-up proteomics and targeted top-down proteomics, we analyzed how the ventricular proteome and sarcomeric subproteome change throughout postnatal mouse heart development (P1, P7, P28, n = 5 per group) and determined the differences in proteome composition in WT and Tnni1 Tg mice (P8 and P28, n = 5 per group). Next, we quantified the differences in MI injury response in WT and Tnni1 Tg mice using a series of measurements, including assessing mitosis markers, cytokinesis markers, and measuring scar formation. Lastly, we conducted a proteomics analysis looking at the injury response in P1 and P7 WT mice and P7 Tnni1 mice 7 days post MI (n = 5 per group).

Results and Discussion: In our global proteomic analysis of postnatal mouse heart development (P1 to P28), we identified a large shift in protein expression from proliferative and developmental processes to an increase in metabolic processes, specifically mitochondrial metabolic processes. During this transition, we also noted that the largest changes in protein expression were isoforms switches in the sarcomere, with the most significant differentially expressed proteins between P1 and P28 hearts being the isoform switch of ssTnI (Tnni1) to cTnI (Tnni3).

With this finding, we explored the differences in baseline proteome composition in WT and Tnni1 Tg mouse hearts. We found that transgenic expression of ssTnI (Tnni1) completely prevented expression of cTnI (Tnni3), and that WT and Tnni1 Tg mice have very similar proteomic profiles. However, we detected a slight shift to a more immature (glycolytic) metabolism in Tnni1 Tg mice based on protein expression.

Next we found that, while injury (MI surgery by permanent ligation of the left anterior descending coronary artery) in P7 WT mice leads to scar tissue formation and cardiac hypertrophy, injury in P7 Tnni1 Tg mice leads to significantly reduced scar formation and complete resolution of the wound through increased CM proliferation, as measured by Mason-Trichrome staining (scar formation), phospho-histone 3 staining (mitosis marker), Aurora B Kinase staining (cytokinesis), and wheat germ agglutinin staining (CM size). These findings indicate that replacement of cTnI with ssTnI promotes cardiac regeneration through CM proliferation.

Lastly, a global proteomic analysis of the molecular processes underlying this increased regenerative capacity of the Tnni1 Tg mice suggests that ssTnI expression conveys a metabolic protection to injury, with increased expression of important proteins involved in metabolic regulation and glycolysis. Thus, these data imply there is a strong link between the sarcomere and metabolism and indicate the isoform switch from ssTnI to cTnI may play a role in the metabolic shift from glycolysis towards fatty acid oxidation that occurs during postnatal development. Future studies are needed to further solidify the role of TnI in metabolism, with the hope that a more comprehensive understanding of this regulation could lead to targeted therapies for treating HF.

Identifying Novel Cardiac Regeneration Enhancers by Utilizing Computational Analyses and Transgenic Assays

Ian J. Begeman[1], Steffani Manna[1], Shikha Vashisht[2], Cecilia Winata[2], Junsu Kang[1]
[1] *Department of Cell and Regenerative Biology, School of Medicine and Public Health, University of Wisconsin–Madison*
[2] *Laboratory of Zebrafish Developmental Genomics, International Institute of Molecular and Cell Biology in Warsaw*

Heart regeneration relies on the reconstruction of gene regulatory networks (GRNs) in response to cardiac injury, which is orchestrated by tissue regeneration enhancer elements (TREEs). Identifying groups of TREEs exhibiting similar features will provide a base for elucidating GRNs that control heart regeneration. We previously dissected a cardiac regeneration enhancer in zebrafish to determine the regulatory mechanisms governing heart regeneration. The cardiac *leptin b* regeneration enhancer (*cLEN*) exhibits injury-inducible activity near the wound in the heart, which is conferred by multiple injury-activated regulatory elements distributed throughout the enhancer. Our analysis also found that cardiac regeneration enhancers are not only activated by injury, but are also actively repressed in the absence of injury, demonstrating dual regulatory mechanisms of cardiac TREEs. Our extensive transgenic assays identified a short 22-bp DNA element containing a key repressive element responsible for maintaining the inactivation of *cLEN* in uninjured hearts. To uncover a group of TREEs similar to *cLEN* present in the genomes of zebrafish, mice, and humans, we devised a strategy to identify *cLEN*-like enhancer candidates by analyzing sequence similarity, evolutionary conservation, target gene functionality, and epigenomic and transcriptomic profiles. Transgenic assays confirmed that multiple predicted enhancers in the zebrafish genome exhibit injury-dependent activation in regenerating hearts. Identifying additional regeneration enhancers across species will expand our understanding of the transcriptional mechanisms underlying heart regeneration and lead to the identification of potential targets for improving heart repair.

Molecular Insights into the 9p21.3 CAD Risk Locus in Diverse Populations

Carolina de Medeiros Vieira, Elsa Salido, Rohan Zade, Parth Parikh, Valentina Lo Sardo
Department of Cell and Regenerative Biology, University of Wisconsin-Madison

Background:
Coronary artery disease (CAD) is the most common form of cardiovascular disease worldwide. It is characterized by atherosclerotic plaque formation, causing the narrowing of the lumen in the coronary arteries, leading to a decreased blood supply to the heart, ultimately causing myocardial infarction (MI). The 9p21.3 locus is the first discovered and the strongest CAD genetic risk factor. Its function is not well understood, perhaps due to the absence of coding genes within it. This locus contains ~100 Single Nucleotide Polymorphism (SNPs) coinherited (forming a haplotype) in the form risk or non-risk in most non-African populations. The risk haplotype at 9p21.3 carried by European ancestry individuals causes transcriptional changes and functional deficits in Pluripotent Stem Cells-derived Vascular Smooth Muscle Cells (iPSC-VSMCs). Interestingly, the 9p21.3 CAD region shows remarkable diversity in individuals of African ancestry, with loss of the characteristic haplotype and lack of linkage with risk of CAD.

Methods:
Cell culture: iPSC maintenance, iPSCs differentiation into VSMCs according to Cheung et. al 2014. *Gene expression:* RNA extraction, cDNA synthesis, RT-qPCR *Immunocytochemistry:* CNN1, TAGLN, α-SMA *Genotyping:* genomic DNA extraction, PCR, Sanger Sequencing *ANRIL overexpression:* lenti-virus production using HEK cells, transfection, infection.

Results:
VSMCs differentiation of iPSCs from African and European ancestry individuals: We generated VSMCs from iPSC lines derived from 2 European (CE, one risk and one non-risk at 9p21.3) and 9 African ancestry (AA) individuals. After 17 days, proper lineage differentiation was validated by immunocytochemistry for typical VSMC markers (CNN1, TAGLN, α-SMA).
Analysis of genes regulating VSMCs adhesion and muscle contraction: RNA from fully differentiated VSMCs was used to perform qPCR for the following genes – ANRIL, FN1, ITGA3, PDLIM1, MYOF, ITGA11, LAMC2, ROBO2, ADAM22, LIMCH1, ITGA9, OBSCN, CDH4.
Analysis of gene expression and SNPs genotype: Cells were genotyped at SNPs in the 9p21.3 locus by PCR and subsequent Sanger sequencing. Gene expression data from iPSC-derived VSMCs were then correlated with the genotype at 9p21.3 of each line.
ANRIL overexpression: AA lines overexpressing ANRIL have genes found to be upregulated in RR cells (LIMCH1, CRABP1, and C1orf61) upregulated.

Discussion:
The VSMCs derived from all CE and AA iPSCs show proper expression of smooth muscle cell markers indicating successful differentiation. Genotyping of SNPs at 9p21.3 showed that the CE lines had a pattern consistent with the linkage disequilibrium in the region, while AA lines showed random pattern across the three alleles. Gene expression data of AA VSMCs suggest a profile similar to non-risk European ancestry lines. A subset of genes shows a pattern of expression correlating with the genotype at 9p21.3 in AA, suggesting a dosage effect of the SNPs at 9p21.3. The use of AA lines with lack of linkage disequilibrium among the SNPs is a great resource to understand allele-dosage dependent gene expression. The overexpression of ANRIL is sufficient to drive the upregulation of few Risk-specific genes in AA lines.

Efficient Sensorless End-to-End Freehand Ultrasound with Physical Inspired Network

Yimeng Dou[1,2], Fangzhou Mu[3], Yin Li[3,4], Tomy Varghese[1,2]
[1]Medical Physics, [2]Electrical and Computer Engineering, [3]Computer Sciences, [4]Biostatistics and Medical Informatics

Background

Three-dimensional (3D) ultrasound (US) imaging is extensively utilized in cardiac, obstetric, abdominal, and vascular examinations. While 3D US with a 'wobbler' transducer suffers from a small field of view and low acquisition rates, freehand scanning offers significant advantages due to its ease of use. However, current 3D US reconstructions methods with freehand scanning are limited by imaging plane shifts along the scanning path (out-of-plane motion). Prior studies have considered incorporating motion sensors; however, they are limited by incurred motion artifacts. A few recent reports have introduced deep neural networks (DNNs) to estimate the relative pose of imaging planes between adjacent frames, but these approaches fall short in handling complex scanning sequences. The goal of this work is to bridge the gap by designing a novel, physics inspired DNN for freehand 3D US reconstruction without motion sensors, to improve reconstruction quality.

Methods

The crux of our approach is to capitalize on the correlation of speckle patterns produced by the interaction between US pulses and tissue microstructure. By tracking speckle across two consecutive frames, our method, realized through a DNN, seeks to estimate the relative pose of the imaging planes. Applying our methods to a sequence of US B-mode frames yields an accurate scanning path and high-quality reconstruction results. This method also eliminates the usage of 3D convolution for extracting spatial-temporal information which significantly reduces computational time for training and inference.

Results/Discussion

Table 1 shows that our method effectively estimates the relative pose between frames (as measured by the distance error, DE) and reduces the drift at the last frame (as indicated by the final drift error, FD), surpassing the strong baseline of DC^2-Net and ConvLSTM. In terms of efficiency, the inference time for DC^2-Net is an average of 4.58 seconds of wall-clock time after 10 runs for a single sequence, and our proposed model is 2.34 seconds. Results were reported on a dataset comprising 128 3D US scans of carotid artery. Due to the limited size of this dataset, transfer learning was employed. All the networks were first trained with 1,928 3D transrectal US scans, in which freehand scans were resampled by generating oblique slices from existing scans. All networks were trained with a Nvidia A40 GPU (Nvidia, USA), using a learning rate of 0.0001, and a batch size of 20. Transfer learning with a learning rate of 0.00001 with 300 epochs as then applied. Further development and comprehensive evaluation of our approach are anticipated.

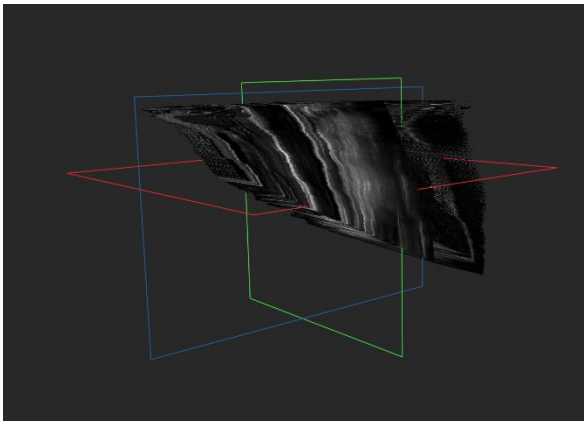

Figure 1. Reconstruction Result.

Table 1.

	DE, med (mm)	DE, max (mm)	DE, min (mm)	DE, avg (mm)	FD, med (mm)	DE, max (mm)	DE, min (mm)	DE, avg (mm)	Wall running time (s)
DC^2-Net	5.10	12.54	3.48	5.94	6.95	20.95	3.39	8.90	4.58
ConvLSTM	4.85	7.20	3.25	4.82	7.22	9.71	5.17	7.35	8.21
Ours	4.32	7.45	3.23	4.47	6.42	10.06	4.66	6.79	2.34

Cerebral Blood Flow Responses to Hyperoxia: Exploring Sex Differences

Travis L. Haley[1], Jessica D. Muer[1], Kaylin D. Didier[1], Brett M. Wannebo[1], Sophie Sanchez[1], Oliver Wieben[2,3], Marlowe W. Eldridge[4], William G. Schrage[1]
[1]*University of Wisconsin-Madison, Department of Kinesiology*
[2]*University of Wisconsin-Madison, Department of Medical Physics*
[3]*University of Wisconsin-Madison, Department of Radiology*
[4]*University of Wisconsin-Madison, Department of Pediatrics*

Background: The administration of oxygen-rich gas (hyperoxia) is a common treatment in clinical medicine and various military occupations. Hyperoxia reduces cerebral blood flow (CBF), however, there exists substantial variability in the magnitude of its effect (0-33%), as well as an uncertainty regarding the role that hypocapnia may play in this vasoconstriction. Interestingly, hyperoxic vasoconstriction appears to be mediated by excessive reactive oxygen species (ROS) signaling. To our knowledge, no studies have directly assessed whether CBF regulation during hyperoxia is sex-specific. This is important since young females are broadly predicted to exhibit lower ROS stress and/or greater antioxidant capacity than males. Therefore, men and women may be differentially impacted. This led us to hypothesize hyperoxia will decrease CBF less in females than males.

Methods: Healthy, young adults (n= 17; 7 F; 20 ± 6 yr; BMI: 20.7 ± 5) were studied after an 8 hour fast and 24 hours without caffeine or alcohol. Women were studied on days 1-5 of menstrual cycle. Subjects completed a single magnetic resonance imaging (MRI) visit. 2D phase contrast (2D PC) MRI was conducted to quantify flow through both internal carotid and vertebral arteries during normoxia, and then repeated during steady-state hyperoxia with subjects breathing 100% O_2. Carbon dioxide (CO_2) was supplemented to maintain end-tidal CO_2 ($ETCO_2$) during hyperoxia. CBF was analyzed as absolute flow (mL/min), total change (∆mL/min), and percent change (% ∆mL/min). In a subset (n=10; 3 F), arterial spin labeling (ASL) MRI was added to explore regional effects on perfusion (mL/100g/min) for an additional 5 mins of hyperoxia. The CAT12 toolbox extension for SPM12 was used to process ASL data. Significance was determined using a two-factor repeated measures ANOVA and was set at $p \leq 0.05$.

Results: Results are mean±SD. Heart rate, mean arterial pressure, and $ETCO_2$ were similar between sexes and did not change between normoxia and hyperoxia ($p>0.05$). When analyzing neck arteries using 2D PC MRI, hyperoxia did not have a significant effect on CBF ($p>0.1$), and there was no differential effect between sexes ($p>0.1$). In contrast, ASL data indicated hyperoxia significantly reduced perfusion in both sexes in all regions analyzed (gray matter, white matter, middle frontal gyrus, frontal operculum, anterior orbital gyrus, superior frontal gyrus, medial frontal cortex, accumbens area, and medial orbital gyrus ($p \leq 0.013$)). There was a trend towards a significantly smaller reduction in females in all regions ($p \leq 0.101$) except the anterior orbital gyrus ($p=0.329$).

Discussion: Contrary to our hypothesis, the CBF response to hyperoxia did not differ between men and women when examining the macrovasculature that supply blood to the brain. However, the smaller hyperoxic reductions in regional perfusion in females indicate that hyperoxia constriction may be sex-specific at the microvasculature level.

Altered Contractile Kinetics in a hiPSC-derived Cardiomyocyte Model of Hypertrophic Cardiomyopathy

Mitchell Josvai[1,2], Alana Stempien[1,2], Willem J. De Lange[3], J. Carter Ralphe[3], Wendy C. Crone[1,2,4,5]

[1]*Departments of Biomedical Engineering, University of Wisconsin-Madison, Madison, WI, USA*
[2]*Wisconsin Institute for Discovery, University of Wisconsin-Madison, Madison, WI, USA*
[3]*Departments of Pediatrics, School of Medicine and Public Health, University of Wisconsin-Madison, Madison, WI, USA*
[4]*Nuclear Engineering and Engineering Physics, University of Wisconsin-Madison, Madison, WI, USA*
[5]*Materials Science and Engineering, University of Wisconsin-Madison, Madison, WI, USA*

Background: Hypertrophic cardiomyopathy (HCM) is a heritable disorder that includes the remodeling and mechanical stiffening of the myocardial walls. As a result, diastolic function is impaired, which may lead to complications including outflow tract obstruction and sudden death. Several mutations are associated with HCM, including those in cardiac myosin binding protein C (cMyBP-C), a regulator of cardiac contractility. Murine models with cMyBP-C ablation have demonstrated alterations in contraction behavior in addition to hypertrophy and fibrosis, but these data are difficult to extrapolate to humans. However, human induced pluripotent stem cell-derived cardiomyocytes (hiPSC-CMs) have recently allowed for the ability model the effects of cMyBP-C knockout on CM contractility and kinetics *in vitro*.

Methods: Wild type (WT), heterozygous and homozygous KO hiPSCs were generated using CRISPR/Cas9-editing. iPSCs were differentiated to CMs and seeded onto either soft (physiological) 10 kPa or stiff (pathological) 40 kPa substrates with micropatterned Matrigel to promote restrictive cell adhesion and 2-dimensional structural organization. On day 6, samples were maintained at 37°C while electrically stimulated (20 V, 0.5 Hz, 2 ms) with contraction behavior recorded on video. Digital image correlation (DIC) was used to quantify contractile strains, and custom MATLAB software was developed to investigate the kinetics of contractile behavior.

Results: On 10 kPa soft PDMS substrates, both heterozygous and homozygous HCM lines demonstrated impaired contractile function and achieved significantly lower magnitudes of strain in comparison to the wild-type control. Conversely, on 40 kPa stiff PDMS substrates homozygous KO samples displayed hypercontractility compared to WT. There were no significant differences in contractile kinetics on 10 kPa substrates. However, WT samples on 40 kPa substrates exhibited significantly faster contractile kinetics than either KO line. The time to reach maximum contraction (CT100) was 52% and 71% longer in heterozygous and homozygous KO, respectively. The time from maximum contraction to a state of 90% relaxation (RT90) was also increased; 89% and 65% for heterozygous and homozygous, respectively. The normalized maximum rates of contraction ($d\varepsilon_2/dt_{max}$) and relaxation ($-d\varepsilon_2/dt_{max}$) were significantly increased on stiff substrates compared to soft substrates for all groups.

Discussion: cMyBP-C is a key regulator of actin-myosin interactions and cardiac contractility. Heterozygous and homozygous KO of cMyBP-C results in decreased strains compared to WT on 10 kPa substrates, while homozygous KOs show hypercontractility on 40 kPa substrates. Both KO lines demonstrated delayed contractile kinetics, requiring increased times to reach maximum states of contraction and relaxation. These data demonstrate that the role of cMyBP-C in hiPSC-CM contraction behavior may be sensitive to environmental cues including substrate stiffness and emphasize the necessity to further investigate the role of these factors in the development of the HCM phenotype.

A Novel ER Compartment as a Substrate for Heteromeric Ion Channel Assembly

Sudharsan Kannan[1], William Kasberg[2], Catherine Eichel[1], Anjon Audhya[2], Gail A. Robertson[1]

1 *Department of Neuroscience, School of Medicine and Public Health, University of Wisconsin–Madison, Madison, WI 53705*

2 *Department of Biomolecular Chemistry, University of Wisconsin-Madison School of Medicine and Public Health, Madison, WI 53706*

Background:
The *human ether-à-go-go related gene* (*hERG*) encodes a potassium channel important for repolarizing the cardiac action potential and modulating neuronal firing. Dysfunction or mutations in hERG cause prolongation in action potential duration, which leads to life-threatening arrhythmias associated with long-QT syndrome, schizophrenia, and epilepsy. Cardiac I_{Kr} is produced by heteromeric assemblies of hERG1a and hERG1b subunits, and depletion of either subunit confers proarrhythmic behavior in cellular cardiac models. hERG 1a and 1b subunits contain identical transmembrane domains and C terminal cytosolic domains, but they contain unique N terminal cytosolic domains. When expressed alone, hERG1a homomers can traffic to the membrane, but hERG1b homomers fail to progress efficiently out of the endoplasmic reticulum (ER). Previously, our lab found that 1b protein contains an RXR motif in its N terminus previously associated with ER retention, and further demonstrated that expressing a part of the N-terminus "masks" the ER retention and inferred that the RXR is masked by 1a while forming 1a/1b heteromers. The mechanisms underlying 1a/1b assembly and the fate of ER-retained channels have not been studied.

Methods:
We used confocal and super-resolution microscopy to study the localization and trafficking of hERG subunits. Quantification of the puncta and colocalization analysis was performed using IMARIS.

Results:
We found that the hERG1b proteins are sequestered and form punctate intracellular structures. When co-expressed with hERG1a, previously shown to promote hERG1b maturation, few puncta are observed, and both signals are robustly present at the plasma membrane. Using confocal and super-resolution microscopy, we show that 1b puncta are primarily localized to the ER and do not overlap with other membranous compartments, including COPII, lysosome, and autophagosome. Localization and pulse-chase experiments show that, in contrast to ER retention and proteasomal degradation of LQT2 mutant proteins, a privileged compartment sequesters and preserves hERG1b subunits. Surprisingly, introducing hERG1a rescued extant 1b from the puncta post-translationally, in contrast to predictions from previous studies.

Discussion:
Sequestration in this novel compartment may limit deleterious homomeric expression of hERG1b and promote heteromeric hERG1a/1b channel assembly post-translationally.

lncRNA Zeb2os Regulates Macrophage Differentiation and Proliferation in Abdominal Aortic Aneurysm

Jooyong Kim[1], Huan Yang[1], Bo Liu[1,2], and Ting Zhou[1],
[1]*Department of Cellular and Regenerative Biology, School of Medicine and Public Health, University of Wisconsin-Madison, Madison, WI 53705, USA*
[2]*Department of Surgery, School of Medicine and Public Health, University of Wisconsin-Madison, Madison, WI 53705, USA*

Background: Macrophages are a critical component of the innate immune system. Uncontrolled macrophage infiltration and accumulation are key pathological characteristics of various vascular diseases, including atherosclerosis and abdominal aortic aneurysm (AAA). Long noncoding RNAs (lncRNAs), which are transcripts longer than 200 nucleotides and lack protein-coding capability, play pivotal roles in normal development and disease pathology. While lncRNAs have been implicated in the pathogenesis of vascular diseases, however, how lncRNAs modulate macrophage functions remains largely unexplored.

Methods and Results: We analyzed published single-cell RNA sequencing datasets from human AAA and several mouse AAA models and discovered a distinct alteration in lncRNA zinc finger E-box binding homeobox 2 opposite strand (Zeb2os in mouse, ZEB2-AS1 in human). Our analysis revealed that Zeb2os was highly enriched in macrophages. To elucidate the role of Zeb2os in macrophages, we isolated bone marrow from C57BL/6J mice and differentiated them into macrophages using 20 ng/ml macrophage colony-stimulating factor (M-CSF), cells were collected 0, 3, and 7 days post bone marrow isolation and subjected to real-time PCR analysis. Compared to Day 0, Zeb2os levels increased as macrophage began to differentiate (Day 3), and subsequently decreased as they reached full differentiation (Day 7). In comparison, the expression of Zeb2, an original strand of Zeb2os, remained elevated throughout the differentiation process. Next, we investigated whether an elimination of Zeb2os would affect the cell proliferation, specifically in an M1-like pro-inflammatory macrophages which is a common phenotype in vascular diseases. The M1-like phenotype was induced by treating Day 7 macrophages with 100 ng/ml lipopolysaccharides (LPS), and the M1-polarization resulted in an elevation of Zeb2os expression. Silencing Zeb2os using various siRNAs revealed a reduction in the expression of the proliferation marker Ki67.

Discussion: Our results suggest that Zeb2os is highly enriched in macrophages and could modulate macrophage differentiation and proliferation. Exploring the role of Zeb2os in macrophages will advance our understanding of vascular inflammation, potentially positioning Zeb2os as a novel therapeutic target for vascular diseases such as AAA or atherosclerosis.

A Computational Model of Pulmonary Artery Stenosis

Callyn J. Kozitza[1], Mitchel J. Colebank[2], Juan Pablo Gonzalez-Pereira[3], Alejandro Roldán-Alzate[1,3,4], and Colleen M. Witzenburg[1,3]

[1]*Dept. of Biomedical Engineering, University of Wisconsin-Madison, Madison, WI*

[2]*Edwards Lifesciences Center for Advanced Cardiovascular Technology and Dept. of Biomedical Engineering, University of California, Irvine, Irvine, CA*

[3]*Dept. of Mechanical Engineering, University of Wisconsin-Madison, Madison, WI*

[4]*Dept. of Radiology, University of Wisconsin-Madison, Madison, WI*

Background: Branch pulmonary artery stenosis (PAS) often presents in children with congenital heart defects, altering blood flow and pressure in the pulmonary circulation during critical periods of growth and development. Variability in PAS onset, duration, and severity result in highly variable growth and remodeling of the large pulmonary arteries, distal vasculature, and the right ventricle. Computational fluid dynamics (CFD) models enable investigation into the hemodynamic impact and altered mechanics associated with PAS. Thus, they have the potential to be used as customizable tools to estimate *in-vivo* tissue remodeling for individualized assessment.

Methods: In this study, a one-dimensional (1D) fluid dynamics model was used to simulate pressure, volumetric flow, and cross-sectional area throughout the pulmonary arteries. The model was fit to previously measured arterial hemodynamics and imaging in 3 swine in which left PAS was surgically created at 2 weeks of age, with 4 additional sham animals. At 20 weeks of age, imaging (CT and 4D Flow MRI), catheterization, and histology were performed. The 1D model was composed of the large pulmonary arteries, whose geometry (length and radius) was specified from animal specific imaging, whereas the distal vasculature (small arteries, arterioles, and capillaries) was represented as a zero-dimensional (0D) lumped parameter model. Remodeling in both the large pulmonary arteries and distal vasculature was estimated by model fitted parameters describing large artery stiffness, total distal vascular resistance, and peripheral compliance.

Results: The main pulmonary artery (MPA) systolic, mean, and diastolic pressures predicted by the model were all within 1% of the measured values and the maximum and time averaged MPA flow produced by the model were within 0.1% of the measured values. In addition, all model predictions of large artery systolic radii were within 4% of the measured values. The model fitted large artery stiffness ranged from 7.1 to 18.5 kPa and was not significantly different between the sham and stenosis groups. The total distal vascular resistance for the sham group suggested a balanced distribution between the left and right sides of the vasculature, whereas the total resistance was generally larger on the left side in the LPA stenosis group. In the sham group, there was a similar peripheral compliance on the left and right side of the vasculature. In contrast, for the LPA stenosis group, the peripheral compliance on the left side was, on average, 2.2-fold lower than the right-side.

Discussion: The model predicted hemodynamics and geometry were in excellent agreement with the measured data for each animal, independent of group. We did not observe a significant difference in large arterial stiffness between the sham and LPA stenosis groups, which may be a consequence of the mild form of stenosis observed in these animals. Histopathological analysis indicated medial hypertrophy in the left small pulmonary arterioles of only the stenosis group animals. This observation independently supports the model fitted reduction in peripheral compliance and increase in resistance observed in the stenosis group. By combining the fitted total distal resistance and peripheral compliance, we used the model further to estimate a ~50% increase in thickness accompanied by a ~10% reduction in radius with no associated changes in stiffness in the left side small arteries/arterioles. Similarly, we estimated an average increase of ~20% in radius of the right side microvasculature with no change in thickness or stiffness. Additional animal studies are necessary to confirm these results.

This study was supported by the AHA and CHF (20CDA35210754) and the NIH (T32HL007936).

Elucidating the Transcriptional and Epigenetic Impact of Succinate Dehydrogenase Inhibition on Cardiac Regeneration

Dakota J. Nuttall[1], Jiyoung Bae[2], Rebecca J. Salamon[1], Wyatt G. Paltzer[1], Timothy J. Aballo[1], Alyssa R. Schuett[1], Ahmed I. Mahmoud[1]

[1]*Department of Cell and Regenerative Biology, University of Wisconsin-Madison School of Medicine and Public Health, Madison, WI, 53705, USA.*

[2]*Department of Nutritional Sciences, Oklahoma State University, Stillwater, OK, 74078, USA.*

Background:

Cardiovascular disease continues to be the number cause of death in the world with myocardial infarction (MI) being the most common pathological cause. Mammalian hearts are limited in their regenerative capacity to recover from damage; however, mice can regenerate after neonatal cardiac injury but cannot after adult cardiac injury. During cardiomyocyte maturation, a metabolic shift from glycolysis towards mitochondrial oxidative phosphorylation takes place. This metabolic shift leads to cardiomyocyte cell cycle exit, suggesting that key metabolic regulators induce transcriptional roadblocks preventing cardiomyocyte proliferation. Our lab recently demonstrated that transient inhibition of succinate dehydrogenase (SDH) by malonate treatment metabolically reprograms the adult heart to a regenerative state by promoting cardiomyocyte proliferation in adult mouse hearts following injury. However, the mechanisms by which cardiac metabolism rewiring affects the transcriptional and epigenetic landscape of adult cardiomyocytes remains unclear.

Methods:

SDH Inhibition and MI Model: 8-week adult male mice are subjected to an MI injury by surgically tying off the left anterior descending artery (LAD) mid-ventricle. Following surgery, mice are injected with either saline or malonate for 14 days, after which the hearts are collected for single nucleus sequencing.

Single Nucleus Multiome Sequencing: Hearts are prepared using the 10x Genomics single-nucleus RNA+ATAC multiome protocol and sent to the UW-Madison Gene Expression Center for sequencing. The raw reads are processed using Cell Ranger and then analyzed with the Seurat R package. Sample data is labeled according to treatment and merged into a single Seurat object for comparison.

Results:

To visualize how SDH inhibition impacts the transcriptional landscape, snRNA-seq data was plotted via UMAP reduction and clustered into all cardiac cell types. As expected, the saline group contained a cluster of activated myofibroblasts, those involved in scar tissue formation after injury. This cluster demonstrated a significant increase in the levels of *Col3a1* and the extracellular matrix component *Bgn*. Remarkably, the activated myofibroblast cluster was absent from the hearts of the malonate-treated mice. This is consistent with the significant reduction in scar size post-MI following malonate treatment, demonstrating that SDH inhibition reduces myofibroblast proliferation and scar formation. To further elucidate how SDH inhibition transcriptionally regulates cardiomyocytes, we performed differential expression between the saline and malonate cardiomyocyte clusters. Interestingly, the malonate cardiomyocyte cluster displayed a significant increase in *Nppb*, a known inhibitor of ventricular fibrosis. Furthermore, there was a significant upregulation of *Malat1* in the malonate cardiomyocyte cluster, which promotes cardiomyocyte proliferation. Additionally, we detected a significant reduction in *Nppa* levels in the malonate cardiomyocyte cluster, which is upregulated during hypertrophy in the control cardiomyocyte cluster. Our preliminary data demonstrates that SDH inhibition not only prevents scar formation, but also promotes a transcriptional landscape conducive to cardiomyocyte proliferation, which are key components of cardiac regeneration.

Discussion:

Metabolic reprogramming through SDH inhibition has been observed to promote adult heart regeneration. This project aims to define the regenerative transcriptional landscape that promotes cardiac regeneration, which may identify novel regulators of adult heart regeneration. Analyzing the snATAC-seq data will reveal the chromatin conformational changes and motifs that contribute to regeneration induced by SDH inhibition. Elucidating the key transcriptional and epigenetic components involved in a metabolically induced adult regenerative model will contribute to the mechanistic underpinning of cardiac regeneration, which one day could uncover novel therapeutics.

Elucidating the role of Mechanistic Target of Rapamycin Complex 1 during Heart Regeneration

Wyatt Paltzer[1], Timothy Aballo[1], Jiyoung Bae[2], Katherine Hubert[1], Dakota Nuttall[1], Kayla Wanless[1], Raya Nahlawi[1], Cassidy Perry[1], Ying Ge[1], Ahmed Mahmoud[1]
[1]Department of Cell and Regenerative Biology, University of Wisconsin-Madison
[2]Department of Nutritional Sciences, Oklahoma State University

Background:
Heart failure is the leading cause of morbidity and mortality worldwide, with no current therapeutic interventions. Stimulation of adult heart regeneration to replace the damaged cardiac tissue has enormous therapeutic potential for treatment of heart failure. In contrast to the adult heart, the neonatal mouse heart demonstrates a remarkable ability to regenerate after injury, which presents a unique model to study the mechanisms that regulate heart regeneration. During cardiomyocyte maturation a metabolic shift occurs, where the primary energy source shifts from glycolysis to fatty acid oxidation, this metabolic shift results in the loss of heart regeneration. Recent work in our lab showed that promotion of glycolysis after adult myocardial infarction injury can promote heart regeneration. Interestingly, a recent study demonstrated that mechanistic Target of Rapamycin Complex 1 (mTORC1) hyperactivity shifted the primary energy source to glycolysis from fatty acid oxidation in the adult heart. However, the role of mTORC1 in heart regeneration is not yet defined. Thus, we hypothesize that mTORC1 will be required for heart regeneration, and hyperactivation of mTORC1 will stimulate adult heart regeneration. Elucidating the role of mTORC1 during heart regeneration will provide key insights on the metabolic regulation during heart regeneration, as well as uncover potential targets for therapeutic intervention to stimulate adult heart regeneration.

Methods:
To examine the role of mTORC1 during heart regeneration I utilized the neonatal mouse myocardial infarction (MI) model. We then analyzed the impact mTORC1 inhibition has during development and injury response by mTORC1 active site inhibition via Rapamycin or Everolimus administration. To identify the mechanism through which mTORC1 inhibition prevents endogenous neonatal cardiac regeneration we conducted proteomic and metabolomic analyses of ventricular tissue to identify cellular changes.

Results:
mTORC1 inhibition during neonatal regeneration prevents the endogenous heart regeneration, resulting in cardiac hypertrophy and scar tissue formation. Proteomic analysis demonstrated that the mTORC1 inhibited hearts relied more upon fatty acid oxidation and oxidative phosphorylation compared to the control hearts. This data was supported in the metabolomic analysis where we observed a shift in the available metabolites due to mTORC1 inhibition. Overall, we demonstrated that mTORC1 is necessary to maintain a glycolytic reliant metabolic state to maintain proper maturation and regenerative capabilities.

Discussion:
Previous literature demonstrates that metabolic state during heart regeneration is key to the promotion or inhibition of heart regeneration. We demonstrated that the function of known metabolic regulator mTORC1 is critical for heart regeneration, with mTORC1 inhibition preventing endogenous heart regeneration. Further examinations are needed to determine the targets downstream of mTORC1 that could eventually be therapeutic targets to stimulate cardiac regeneration after adult injury.

Hemodynamics in Coarctation of the Aorta using 4D Flow MRI, Computational Fluid Dynamics, and Particle Image Velocimetry

James Rice[1], Labib Shahid[1], Alejandro Roldan-Alzate[1,2]
[1]*Department of Mechanical Engineering, University of Wisconsin-Madison*
[2]*Department of Radiology, University of Wisconsin-Madison*

Background: Coarctation of the aorta (COA) is one of the most common congenital heart defects. It is characterized by a narrowing in the aortic arch or proximal descending aorta. The selection criteria for the optimal treatment strategy are not well defined and post-intervention complications due to sub-optimal repair are common. 4D Flow MRI is a diagnostic imaging technique capable of measuring time-resolved 3D blood velocities within a volumetric acquisition region. 4D Flow MRI has potential to be used as a tool for treatment planning, however, imaging on its own provides no predictive capabilities. To overcome this challenge, image-based computational fluid dynamics (CFD) and in vitro modeling can be used as predictive tools that enhance 4D Flow MRI for COA treatment planning. To validate this predictive technique in the case of COA, we analyzed 4D flow MRI and CFD data using in vitro tomographic (3D) particle image velocimetry (PIV) flow experiments.

Methods: In-vivo 4D Flow MRI was performed in four pediatric patients before and after COA repair following an IRB-approved HIPAA-compliant protocol. The thoracic aorta was segmented and flow rates at the ascending aorta, brachiocephalic, left common carotid, left subclavian arteries, and descending aorta were obtained. 4D Flow MRI was used to generate anatomical aorta models that were used to produce realistic MR-compatible flow phantoms via additive manufacturing. The flow rate in the ascending aorta was imposed and the flow rates in the distal arteries were measured. The flow rates from CFD and PIV were compared against in vivo 4D Flow MRI for validation.

Results: One patient was presented with a mycotic aneurysm that was not visualized by 4D Flow MRI. Two patients underwent stenting and 4D Flow MRI could not acquire the in-stent blood flow. Both CFD and PIV successfully visualized and quantified aneurysmal and in-stent hemodynamics. Flow rates calculated by CFD agree with 4D Flow MRI within 10%. Different flow dynamics metrics calculated with all methodologies were compared for all the cases.

Discussion: 4D flow MRI is used in computational and in vitro experimentation by providing the anatomical and in vivo flow information necessary to drive patient-specific modeling. Image-based CFD and in vitro modeling can be used to complement 4D flow MRI, such as virtually testing and simulating interventions. For all patients, CFD- and PIV-derived hemodynamics suggest that COA-repair strategies successfully reduce peak velocities at the site of the repair and work to restore normal aortic blood flow.

Comprehensive Characterization of Endogenous Phospholamban Enabled by Top-Down Proteomics and Photocleavable Surfactant

Holden Rogers[1], David S. Roberts[1], Eli Larson[1], Jake Melby[1], Kalina Rossler[2], Austin Carr[1], Kyle Brown[1,3] and Ying Ge[1,4,5]

Department of Chemistry[1]; Department of Molecular and Cellular Pathology[2]; Department of Surgery[3]; Department of Cell and Regenerative Biology[4]; Human Proteomics Program[5], University of Wisconsin-Madison, WI

Background: Phospholamban (PLN) is a regulatory transmembrane protein in the sarcoplasmic reticulum; its interaction with Ca^{2+}-ATPase SERCA2a is essential in Ca^{2+} handling and cardiac contractility. The function of PLN is dynamically regulated by multiple post-translational modifications (PTMs). Phosphorylations on Ser16 and Thr17, regulated by protein kinase A and Ca2+/calmodulin-dependent protein kinase II, respectively, are key contributors to PLN's regulatory role in muscle contraction. S-palmitoylation on Cys36 by an acyltransferase has been implicated both in the enhancement of phosphorylation on Ser16 and pentamer formation once PLN is phosphorylated. The ability to investigate the presence or absence of PLN modifications directly from human cardiac tissue will be crucial to better understanding PLN's role in disease. Therefore, it is essential to develop an analytical method capable of comprehensively characterizing PLN's combinatorial PTMs.

Methods: Proteins were extracted from ~15 mg of cryopulverized ventricular tissue from human donor hearts using a two-stage extraction at 4 °C. Cytosolic proteins were depleted twice with an ammonium bicarbonate buffer. After centrifugation, the pellet was homogenized in an Azo buffer to solubilize membrane proteins, including PLN. Extracted proteins were buffer exchanged using methanol/chloroform/water precipitation and resolubilization. Samples were then UV-irradiated to degrade any remaining Azo. To characterize PLN, we employed a two-pronged top-down MS approach using an online reversed-phase liquid chromatography tandem MS method on a quadrupole time-of-flight MS and a direct infusion method via an ultrahigh-resolution Fourier-transform ion cyclotron resonance MS. DataAnalysis (ver. 4.3; Bruker Daltonics) and MASH Native (ver. 1.1) software were used to process and analyze the LC-MS/MS data.

Results and Discussion: The highly reproducible and robust top-down proteomics platform resulted in the simultaneous identification and fragmentation of various PLN proteoforms. This novel top-down MS-based approach enabled comprehensive PTM mapping of PLN, including the localization of S-palmitoylation to Cys36 and the site-specific localization of phosphorylation to Ser16 and Thr17 by MS/MS for the first time. We then applied our methodology to examine PLN in the disease state and reported the significant decrease in phosphorylation of PLN in human failing hearts with ischemic cardiomyopathy, a predominant form of heart failure. These findings agree with previous literature indicating that reduced Ca^{2+} cycling in failing hearts is associated with hypophosphorylation of PLN, as unphosphorylated PLN inhibits SR Ca^{2+}-ATPase 2a activity. Overall, this targeted top-down MS method will be highly valuable for understanding the regulatory roles of combinatorial PTMs of PLN in cardiac contractility and disease.

Integrated Proteomics Analysis of *In Vitro* Hypertrophic Cardiomyopathy Models

Kalina J. Rossler[1], Willem J. de Lange[2], Jake A. Melby[3], Morgan W. Mann[4], Timothy J. Aballo[1], Jianhua Zhang[4], Gina Kim[4], Yanlong Zhu[5], Emily Farrell[4], Timothy J. Kamp[1,4], J. Carter Ralphe[2], and Ying Ge[1,3,5]

[1]*Department of Cell and Regenerative Biology, University of Wisconsin-Madison*
[2]*Department of Pediatrics, University of Wisconsin-Madison*
[3]*Department of Chemistry, University of Wisconsin-Madison*
[4]*Department of Medicine, University of Wisconsin-Madison*
[5]*Human Proteomics Program, University of Wisconsin-Madison*

Background: Hypertrophic cardiomyopathy (HCM) is the leading cause of sudden cardiac death in young adults. Nearly 1,500 HCM-related mutations in sarcomeric genes have been identified, but the molecular events leading to the disease phenotype remain largely unknown. While previous studies have focused on functional and transcriptional changes in HCM-specific human induced pluripotent stem cell-derived cardiomyocyte (hiPSC-CMs) models, comprehensive characterization of proteome changes in regards to functional phenotype has yet to be explored.

Methods: Herein, we have generated 2D (monolayer) and 3D (engineered cardiac tissues; ECTs) hiPSC-CM models from family members with no mutation and an HCM-causing β-myosin heavy chain (*MYH7*) R663H mutation to be evaluated via mass spectrometry (MS)-based proteomics.
For 3D ECTs, isometric twitch force meaurements were performed to characterize contractile performance. Using the same ECTs, proteins were extracted and analyzed using integrated liquid chromatography-mass spectrometry (LC-MS)-based approaches to obtain a “bird’s eye view” of the sarcomere sub-proteome to quantify changes in PTMs as well as a whole-proteome profiling of protein expression.

Results: Functional measurements showed HCM models displayed aberrant calcium handling and elongated twitch force curves to the control group. Intact sarcomere protein analysis revealed differential expression of myosin light chain 2 (MLC-2) isoforms in monolayer cultures ($p<0.01$), mirroring the upregulation of the ventricular isoform observed for HCM manifestation *in vivo*. Furthermore, our HCM ECT models uncovered significant decreases in total phosphorylation for contractile proteins MLC-2v and alpha-tropomyosin compared to controls. Global bottom-up proteomics data determined that extracellular matrix (ECM) proteins such as collagen I were downregulated in both disease models. Along with key hypertrophic factors, proteins involved in glucose metabolism were upregulated in the HCM samples.

Discussion: These results revealed altered function and proteoform landscape in both monolayer and ECT HCM models. Indeed, our work to integrate functional and molecular parameters in “early stage” HCM constructs provides mechanistic insight into the progression of cardiac disease.

9p21.3 Coronary Artery Disease Risk Locus and Vascular Function

Elsa Salido, Carolina de Medeiros Vieira, Huang Yang, Valentina Lo Sardo
Department of Cell and Regenrative Biology

Background: Coronary Artery Disease (CAD) is the primary cause of death worldwide. Although it is traditionally associated with environmental factors like dietary and exercise choices, CAD has a strong genetic component, being 40-60% heritable. More than 300 loci have been linked to CAD, but the most impactful is a 60 Kb gene desert haplotype in the 9p21.3 locus. This region contains ~80 Single Nucleotide Polymorphisms (SNPs) in high linkage disequilibrium in most populations, which produce two haplotypes: one which is associated with increased risk of CAD, and one which is not. Although it contains no genes, this region overlaps partially with a lncRNA gene called ANRIL. Previously, we showed that iPSC-derived VSMCs from individuals with the risk haplotype exhibit ~3000 differentially expressed genes, including other CAD-related genes. Deletion of the risk haplotype rescues this phenotype, suggesting that it confers a gain of function. Specific isoforms of the lncRNA ANRIL were enriched in the risk cells, and overexpression of these isoforms in non-risk cells partially recapitulated the risk phenotype. Here, we present a single cell RNA sequencing analysis of iPSC-derived VSMCs with the risk or non-risk backgrounds, as well as isogenic knock-outs in both backgrounds.

Methods:
Cell culture: iPSC maintenance, iPSCs differentiation into VSMCs according to Cheung et. al 2014.
Single-cell sequencing: 10x genomics 3' scRNAseq
Computational analysis: Principle component analysis, Louvain clustering, and differential expression analysis (R studio 4.2.1, Seurat V4), Gene ontology (PANTHER classification system), comparison of genetic expression to published datasets (Wirka et al. 2019, Hu et al. 2021)

Results: Our analysis reveals that the risk haplotype at 9p21.3 causes VSMCs to acquire an aberrant cell fate that does not recapitulate known disease states of VSMCs. Instead, this aberrant state exhibits a tendency toward multiple non-SMC lineages, suggesting novel cellular pathways playing a role in CAD risk. We also identified a set of genes exclusively expressed in risk VSMCs which may drive the risk phenotype. We show that the expression of these genes is modulated by the expression of ANRIL isoforms exclusively expressed in risk cells.

Discussion: This study suggests a new role for the 9p21.3 CAD risk locus in determining cell fate in VSMCs and may uncover new cellular processes acting in CAD. Additionally, the genes identified here are novel downstream effectors of 9p21.3, providing new insights into cellular events that lead to 9p21.3-mediated CAD risk.

Gestational Intermittent Hypoxia-Induced Endothelial Dysfunction and Hypertension in Pregnant Rats: Evidence for a Role of Endothelin Type B Receptor

Ruolin Song[1], Pankaj Yadav[1], Sri Vidya Dangudubiyyam[2], Alissa Hofmann[2], Jay S. Mishra[1], and Sathish Kumar[1,2]

[1] *Department of Comparative Biosciences, School of Veterinary Medicine, University of Wisconsin-Madison, WI*

3 *Department of Obstetrics and Gynecology, School of Medicine and Public Health, University of Wisconsin-Madison, WI*

Background: Obstructive sleep apnea (OSA) is a recognized risk factor for gestational hypertension, yet the exact mechanism behind this association remains unclear. Here, we tested the hypothesis that intermittent hypoxia (IH), a hallmark of OSA, induces gestational hypertension through perturbed endothelin-1 signaling.

Methods: Pregnant Sprague–Dawley rats were exposed to normoxia (control), mild IH (mIH, 10.5% O_2), or severe IH (sIH, 6.5% O_2) from gestational day (GD) 10 to 21. Blood pressure (BP) was monitored though GD 17 to 20. At the end of the study (GD 21), plasma was collected and mesenteric arteries were isolated for myograph and protein analyses.

Results: 1) Pregnant rats exposed to mIH or sIH had higher BP, lower plasma nitrate/nitrite (NOx) levels, and unchanged endothelin-1 levels compared to control rats. **2)** Western blot analysis showed that mIH and sIH exposure decreased the expression of endothelin type B receptor (ET_BR) and phosphorylated endothelial nitric oxide synthase (eNOS), while the levels of endothelin type A receptor (ET_AR) and total eNOS remained unchanged. **3)** The contractile responses to potassium chloride, phenylephrine, and endothelin-1 were not affected in endothelium-denuded arteries from mIH and sIH rats. However, mIH and sIH rats had impaired endothelium-dependent vasorelaxation responses to the ET_BR agonist IRL-1620 and acetylcholine compared to controls. Endothelium denudation abolished IRL-1620-induced vasorelaxation, supporting the involvement of the endothelium in ET_BR-mediated relaxation. **4)** Treatment with IRL-1620 through systemic infusion during GD 14-21 significantly attenuated IH-induced hypertension in pregnant rats. This was associated with increased circulating NOx levels, enhanced ET_BR expression, increased eNOS activation, and improved vasodilation responses.

Discussion: Our data suggest that IH exposure during gestation increases BP in pregnant rats by suppressing ET_BR-mediated signaling. This establishes a molecular mechanism linking IH to gestational hypertension. The stimulation of ET_BR signaling through pharmacological agonists emerges as a promising therapeutic approach for managing gestational hypertension associated with OSA.

9p21.3 CAD Risk Locus and mRNA Regulation

Shraddha Suryavanshi, Elsa Salido, Valentina Lo Sardo
Department of Cell and Regenerative Biology, University of Wisconsin-Madison

Background:
Cardiovascular disease (CVD) is the leading cause of death in the U.S. and worldwide. Coronary artery disease (CAD) is the most common kind of CVD and accounts for almost 50% of cardiovascular deaths. Around 300 genomic loci have been linked to increased risk of CAD, and the most impactful is a 60 kb region at the 9p21.3 locus**.** This region is a gene desert containing 80 single nucleotide polymorphisms (SNPs) in linkage disequilibrium in most populations, which form a haplotype in a risk and non-risk form. Previously, we showed that induced pluripotent stem cells (iPSCs)-derived Vascular Smooth muscle Cells (VSMCs)) from individuals carrying the risk haplotype at 9p21.3 acquire a unique phenotypic transition not resembling the typical contractile-to-synthetic state. Bulk RNA sequencing analysis showed ~3000 differentially expressed genes (DEGs) in risk VSMCs when compared to non-risk ones. Both single cell and bulk RNA sequencing analyses show upregulation of biological processes related to mRNA processing and RNA splicing, pointing to mRNA regulation as a potentially critical factor in 9p21.3 locus-mediated CAD risk.

Methods:
Cell culture: iPSC maintenance, iPSCs differentiation into VSMCs according to Cheung et. al 2014. *Computational:* Principal Component analysis, Louvain clustering, and differential expression analysis (R studio 4.2.3, Seurat V4, DESeq2 R package v1.8.2), Gene ontology analysis (PANTHER classification system)

Results:
Gene ontology analysis was performed on the differentially expressed genes (DEG) identified in our bulk RNA sequencing analysis comparing risk VSMCS to the isogenic risk knockout, non-risk VSMCs, and isogenic non-risk knockout. The gene ontology terms related to RNA splicing, mRNA splicing via spliceosome, mRNA metabolic processes, and mRNA processing showed greater fold enrichment compared to the other biological processes. We merged the lists of genes associated with these four to generate a list of 135 splicing related genes. We then ranked the genes by fold change, and the top 10 genes were selected for further analysis. We performed the same analysis with single cell RNA seq data and the top 20 genes by fold change related to splicing were selected. We analyzed the expression of the genes from both the bulk and scRNA analysis and found they all exhibited unique expression patterns in the risk VSMCs relative to isogenic knockouts and non-risk cells. In total, 30 mRNA splicing related genes of interest were identified as a part of the risk phenotype.

Discussion:
The findings presented here provide support for a possible role of the 9p21.3 CAD risk region in the regulation of mRNA splicing. Our gene ontology results suggest that mRNA splicing regulation is a significant part of the risk phenotype. Recent literature provides insights on the link between proper splicing genes expression and potential risk for CAD. The 30 splicing genes we identified may be downstream effectors of 9p21.3, potentially providing insight into the cellular events regulating 9p21.3-mediated CAD risk.

Neutral Sphingomyelinase Mediates Phenotypes of Cardiac Hypertrophy

Daniel G. P. Turner[1], Willem J. De Lange[2], Yanlong Zhu[3], Ying Ge[3], Timothy J. Kamp[1], J. Carter Ralphe[2], Alexey V. Glukhov[1]

Departments of Medicine[1], Pediatrics[2], and Chemistry[3], University of Wisconsin-Madison, USA

Background: Hypertension is a risk factor for heart failure and arrhythmias, where chronically elevated myocardial stretch in hypertensive patients is considered a crucial contributor to pathological cardiac remodelling. We hypothesized that neutral sphingomyelinase (nSMase), a mechanosensitive membrane hydrolase enzyme, is activated during chronic stretch which generates inflammatory ceramides and disrupting plasma membrane morphology, leading to myocardial remodelling.

Methods: We utilized human engineered cardiac tissue (ECT) composed of human-induced pluripotent stem cell-cardiomyocytes and -fibroblasts, to develop a chronic cyclic stretch protocol. Effects of stretch-induced nSMase activation were assessed on cardiomyocyte plasma membrane morphology, ECT contractility and response to sympathetic stimulation as well as expression of fibrotic mRNAs and generation of ceramide and H_2O_2. Optical mapping of action potentials was also used to determine electrophysiological effects of acute nSMase mechano-activation in *ex vivo* Langendorff-perfused mouse hearts.

Results: Cyclic stretch recapitulated phenotypes of pathological cardiac remodelling, which included increased membrane tension, reduced caveolae abundance, blunted β-adrenergic response, and an increase in ceramide production and fibrotic mRNAs. nSMase inhibition by GW4869 prevented all these effects, without affecting stretch-induced membrane tension. We also observed an nSMase-independent upregulation of *ACTA2* and *COL3A1* mRNA and H_2O_2 production in response to stretch. In *ex vivo* mouse heart experiments, acute ventricular stretch resulted in nSMase-mediated conduction slowing, further supporting stretch-induced activation of nSMase in native myocardium.

Discussion: Overall, we utilize advanced stem cell and tissue engineering techniques, complemented by mouse heart studies, to produce a novel *in vitro* stretch protocol that recapitulates phenotypes of cardiac pressure overload and identify nSMase as stretch-induced regulators of cardiac remodelling that is associated with hypertension.

Angiotensin Type 2 Receptor Activation Reverses PFOS-Induced Uterine Vascular Hyper-Reactivity and Hypertension in Pregnancy

Sri Vidya Dangudubiyyam[1, 2], Bradley Bosse[3], Pankaj Yadav[1], Ruolin Song[1]; Alissa Hofmann[1, 2], Jay S. Mishra[1], Sathish Kumar[1, 2, 3*]

[1]Department of Comparative Biosciences, School of Veterinary Medicine, University of Wisconsin, Madison, WI 53706, USA.

[2]Endocrinology-Reproductive Physiology Program, University of Wisconsin, Madison, WI 53715, USA.

[3]Department of Obstetrics and Gynecology, School of Medicine and Public Health, University of Wisconsin, Madison, WI 53792, USA.

Background: Preeclampsia, a hypertensive disorder of pregnancy, poses significant risks to both maternal and fetal health. There is currently no effective treatment for preeclampsia, largely due to the unclear pathophysiological mechanisms. Recent scientific investigations have uncovered a compelling association between exposure to perfluorooctane sulfonic acid (PFOS) in the environment and the development of preeclampsia. Our studies have demonstrated that PFOS exposure during pregnancy induces hypertension in pregnant rats with associated decreased vasodilatory angiotensin type-2 receptor (AT2R) expression and impaired vascular reactivity in uterine arteries, resulting in reduced fetal weights. Clinical studies also show that AT2R protein was reduced in preeclamptic placental vessels. We hypothesized that AT2R activation would improve PFOS-induced maternal syndrome and fetal outcomes.

Methods: Pregnant Sprague-Dawley rats were exposed to PFOS through drinking water (50 μg/mL) from gestation day (GD) 4─20. Controls received drinking water with no detectable PFOS. A subset of control and PFOS-exposed rats were treated with AT2R agonist Compound 21 (C21; 0.3 mg/kg/day, SC) from GD 15─20. On GD 20, non-invasive blood pressures, Doppler blood flow, and endothelium-dependent and –independent vascular reactivity with wire myograph, AT1R, AT2R, and eNOS protein abundance, plasma bradykinin levels, and fetoplacental weights were assessed.

Results: PFOS dams exhibited elevated systolic, diastolic, and mean arterial blood pressure, and administration of AT2R agonist C21 prevented PFOS-induced increase in blood pressure. PFOS dams demonstrated a significant reduction in uterine artery blood flow, accompanied by increased resistance and pulsatility indices compared to the control group. Administration of C21 significantly restored uterine artery blood flow and normalized resistance and pulsatility indices to control levels. C21 attenuated the exaggerated Angiotensin II (Ang II) mediated contraction and improved endothelium-dependent vasorelaxation responses to acetylcholine in uterine arteries of PFOS dams. These C21-mediated vascular effects were associated with decreased AT1R, increased AT2R, and eNOS protein levels. C21 also increased plasma bradykinin production in PFOS dams and attenuated the fetoplacental growth restriction.

Discussion: These data suggest that C21 improves the PFOS-induced maternal vascular dysfunction and blood flow to the fetoplacental unit, providing preclinical evidence to support the hypothesis that AT2R activation may be an important therapeutic target for the treatment of PFOS-induced adverse maternal and fetal outcomes.

Roundabout Receptors are Required for Maintaining Islet Architecture during Acute Pancreatitis

Matthew R. Wagner[1], Bayley J. Waters[1], Barak Blum[1]
[1]*Department of Cell and Regenerative Biology*

Background:
Acute pancreatitis (AP) is an inflammatory condition that leads to dysregulated islet-hormone secretion and glucose homeostasis as inflammation and systemic insulin resistance increase[1]. Although glucose metabolism is known to be dysregulated during AP, the exact mechanism remains unknown.

Pancreatic islets are highly vascularized clusters of endocrine cells that regulate blood glucose levels throughout life by coordinating insulin and glucagon release. Islet cells preferentially organize with homotypic over heterotypic interactions, with a core of β cells and a mantle of α and δ cells. Evidence suggests that proper organization is necessary for accurate and appropriate hormone secretion. Development and maintenance of this islet architecture partially involves the expression of Roundabout receptors (Robo) in β cells and Slit expression in the mesenchyme[2,3]. We hypothesized that islet architecture is disturbed in RoboKO mice in response to AP.

Methods:
To test this hypothesis, we conditionally deleted Robo2 in β cells of three adult mice and used immunofluorescence to observe islet architecture following the induction of acute pancreatitis. Quantifications of α and δ cell number and location were done using Fiji.

Results:
We show that inducing AP in adult RoboKO mice results in disrupted islet organization when compared to wild-type controls. The islets of RoboKO mice present with a significant increase of α and δ cells found within the β cell core, with no change in the percent of α and δ cells to total cells.

Discussion:
These data suggest that Robo2 plays a role in stabilizing islet architecture during pancreatitis and further supports previous studies that Robo2 is necessary for the coordinated expansion of islets. Understanding the maintenance and expansion of islet architecture is critical for developing therapies for islet-associated conditions like diabetes. Future experiments using RoboKO mice will reveal the impacts of aberrant architecture on glucoregulation during pancreatitis recovery.

References:
[1]Yi, Y., et al *Pancreatology* 2021. [2]Adams, M. T., et al *Scientific Reports* 2018. [3]Gilbert, J. M., et al *Molecular and Cellular Biology* 2021.

Evaluation of Multiple Extraction Methods for the Analysis of Human Heart Metabolites

Benjamin Wancewicz[1, 2], Melissa R. Pergande[1], Yanlong Zhu[1,2], Zhan Gao[1], Zhuoxin Shi[1], Kylie Plouff[1], Ying Ge[1,2]

[1] Department of Cell and Regenerative Biology, University of Wisconsin-Madison, Madison, WI
[2] Human Proteomics Program, University of Wisconsin-Madison, Madison, WI

Background: The heart contracts incessantly to supply oxygenated blood to the entire body and thus, requires a constant source of energy to fuel its high energy demands. The heart is a “metabolic omnivore” and utilizes a variety of fuel substrates, ranging from very polar (e.g., amino acid and nucleosides) to very non-polar (e.g., lipids). Therefore, a comprehensive metabolomic analysis is critical to understand cardiac metabolism; however, it remains challenging as the broad range of metabolite polarities makes extraction and detection difficult. Utilizing multiple extractions ensures we can enrich across the broad range of metabolite polarities. Multiple mass spectrometry (MS)-based platforms can be used for the analysis of metabolites, each having its own unique advantage. Herein, we implemented parallel extractions and mass spectrometry for a comprehensive metabolomic analysis of the human heart.

Methods: Left ventricle tissue from healthy donor tissue was dissected, snap frozen in liquid nitrogen, and cryopulverized prior to extraction. Metabolites (polar metabolites and lipids) were extracted using multiple solvent mixtures including monophasic (100% methanol, 80% methanol and 3:3:2 acetonitrile: isopropanol: water), biphasic (Matyash and Bligh and Dyer) and triphasic (3 phase liquid extraction, 3PLE) extraction methods; all extractions were done in triplicate. Extracted metabolites were analyzed using ultrahigh-resolution direct infusion Fourier-transform ion cyclotron resonance (DI-FTICR) MS, and high-resolution Fourier-transform ion cyclotron resonance MS (LC-Q-TOF MS/MS). Raw mass spectrometry data was analyzed where metabolic features were extracted and annotated. Further, metabolite classification and pathway analysis were performed to determine biological relevance.

Results: Using DI-FTICR MS, 9,521 metabolic features were detected where 7,699 were assigned a chemical formula and 1,756 were assigned an annotated by accurate mass assignment. Using LC-Q-TOF MS/MS, 626 metabolites were identified based on fragmentation matching against publicly available libraries. Collectively, 2276 heart metabolites were identified in this study which span a wide range of polarities including polar (benzenoids, alkaloids and derivatives and nucleosides) as well as non-polar (phosphatidylcholines, acylcarnitines, and fatty acids) compounds. These included both previously reported and newly identified human heart metabolites. Additionally, pathway analysis of identified metabolites revealed increased coverage by using this comprehensive approach compared to any single extraction alone. Together, multiple parallel extractions and mass spectrometry platforms outperform any single approach.

Discussion: Herein, we describe a comprehensive analysis of the human heart metabolome where six parallel liquid-liquid extraction methods (three monophasic, two biphasic, and one triphasic) and two complementary MS-based detection platforms (DI-FTICR and LC-QTOF MS/MS) were utilized. With this approach, we measured key metabolites in heart function, as well as identified new metabolites in the human heart. We envision that the information in this study may be useful in selecting an appropriate extraction and MS detection platform to assist in metabolomic analyses of the human heart.

Structure-Function Analysis of Two Novel Calcins Based on a Transcriptomic Comparison of East Asian Scorpions

Li Xiao[1,2], Xiaoyu Hua[3], Jun Li[3,4], Fengling Yang[5], Songyu Gao[3], Carmen R Valdivia[1], Jinchi Yao[3,6], Wenxuan Cai[1], Zhixiao Yang[3,7], Liang Xiao[3], Héctor H Valdivia[1]

[1] *Cardiovascular Research Center, University of Wisconsin – Madison.*

[2] *Sichuan University, Chengdu, China.*[3] *Naval Medical University, Shanghai, China.*

[4] *Shanxi Agricultural University, TaiGu, China.*

[5] *Jilin Agricultural University, Changchun, China.* [6] *Liaoning Normal University, Dalian, China.*[7] *Yunnan University of Chinese Medicine, Kunming, China*

Background: Calcins are a family of membrane-penetrating peptides from scorpion venom that target the intracellular Ca^{2+} release channel/ryanodine receptor (RyR) with high affinity and specificity. Dysfunction of RyRs plays a critical role in several diseases of skeletal and cardiac muscle, but there are not yet in the market effective pharmacological therapies to control their activity. Imperacalcin (IpCa, previously kown as Imperatoxin A), the founding member of calcins, binds to RyRs with nanomolar affinity and induces a long-lived subconductace state that in cardiac muscled may prevent SR Ca^{2+} overload-induced arrhythmias. IpCa spawned the discovery of other members of the calcin family, including Maurocalcin, Opicalcin, and others. East Asian scorpions are a rich source of toxins, peptides, and other active components but the presence of calcins is not clear.

Methods: We investigated *de novo* transcriptomes from scorpion venomous glands from 10 East Asian regions. Species identification, toxin screening, molecular docking, and molecular dynamic simulation were conducted subsequently.

Results: We identified two species, Uroctonus mordax and Mesobuthus martensii, that shared a total of 1,358 toxins among the 2,451 transcriptome-screened toxins. However, U. mordax has a significantly larger number of unique toxins compared to M. martensii. In this set, we discovered two novel calcin peptides, Urocalcin-M1 and Urocalcin-M2, that share 72.7% sequence similarity. Similar to other calcins, Urocalcin-M1 and Urocalcin-M2 are folded by the characteristic inhibitor cysteine knot motif, are rich in basic amino acids, have high affinity for RyR1 and induce a sub conductance state in RyR1. Molecular docking and molecular dynamic simulation predicted that they both bind to the channel domain of RyR1 in an open state. Urocalcin-M1 has a higher affinity than M2, however, M2 induces longer sub conductance state. Lysine11 is a key amino acid residue that affects the affinity difference between these two calcins. Moreover, the substitution of residues at positions 2 and 4 of M1 with residues at the same position of M2 improves the binding affinity of M1.

Discussion: We speculate that geographic difference between scorpions U. mordax and U. martensii provides an explanation for the variation of toxicity and pharmacological activity of these scorpion peptides from East Asian regions. The discovery of Urocalcin-M1 and M2 from U. mordax enriches the sequence and structural diversity of the calcin family.

Extracellular Vesicles and Abdominal Aortic Aneurysm

Qianfan Yang[1], Jack Bontekoe[2], Jooyong Kim[1], Huan Yang[1], Ting Zhou[1], Zulmari Silva-Pedraza[3], Bo Liu[1.2]

[1]Department of Cellular and Regenerative Biology, School of Medicine and Public Health, University of Wisconsin-Madison, Madison, WI 53705, USA

[2]Department of Surgery, School of Medicine and Public Health, University of Wisconsin-Madison, Madison, WI 53705, USA

[3]Department Materials Science & Engineering, College of Engineering, University of Wisconsin-Madison, Madison, WI, 53705, USA

Background:

Necroptosis, a form of programmed cell necrosis, plays an important role in pathogenesis of multiple common human diseases including atherosclerosis and aortic aneurysm. Prior work in our lab on mouse embryonic fibroblasts (MEFs) has also shown that cells increase their production of extracellular vesicles (EVs) in response to necroptosis signaling. Additionally, EVs derived from necroptotic MEFs contain a greater variety of proteins which are unique to those from non-necroptotic MEFs. However, there is a limited understanding of how EVs influence inflammation in aortic aneurysm. In this study, we hypothesized that the major constituents of the aortic wall, vascular smooth muscle cells (VSMCs), produce a greater number of EVs in response to necroptosis, which influence adjacent naïve cells toward a pro-inflammatory phenotype.

Methods: Commercially available mouse vascular smooth muscle cells (MOVAs) were used in this study. To test EV production in response to necroptosis over time, MOVAs were treated with zVAD (a caspase inhibitor) and TNFα for 2hrs, 4hrs and 6hrs. EVs were then isolated from the conditioned cell media by differential centrifugation and evaluated by nanoparticle tracking analysis (NTA). Naïve MOVAs were cocultured with necroptotic-derived EVs for 24 hours, then accessed by qPCR for transcriptional changes.

Results: SMCs produce more EVs ---in a time dependent manner --- in response to necroptosis, which is consistent with our previous findings made in MEFs. Treatment with necroptotic EVs caused naïve SMCs to increase the expression of pro-inflammatory gene (IL6, CCL2, IL1β and TNFα) expression, compared to those treated with control EVs, suggesting a phenotypic switch toward inflammation. We began to determine the unique EV cargo(s) that is responsible for the pro-inflammatory function of necroptotic EVs by analyzing our prior mass spectrometry data from MEF-derived EVs. We found that Cav1, a protein involved with EV loading of miRNA, is highly enriched in EVs from necroptotic MEFs.

Discussion: Our data demonstrates a positive correlation between necroptosis and EV production in both MEFs and SMCs. Our co-culture experiment demonstrates that necroptotic EVs are capable of inducing proinflammatory responses in naïve SMCs, which may help to explain phenotype switch of SMCs seen within the aneurysmal tissues. Our next steps aim to test whether Cav1 mediates the pro-inflammatory function of necroptotic EVs.

The 9p21 Risk Locus Controls Cell Motility in Vascular Smooth Muscle Cells

Rohan Zade, Carolina de Medeiros Vieira, Elsa Salido, Isaac Zhang, Parth Parikh, Valentina Lo Sardo
Department of Cell and Regenerative Biology, University of Wisconsin-Madison

Background:
Coronary artery disease (CAD) is the most common form of cardiovascular disease. The 9p21.3 locus was the first genomic locus to be linked to CAD and remains the strongest genetic association. Vascular smooth muscle cells (VSMCs) are one of the major components of the coronary arteries. Their migration capacity plays a major role in atherosclerotic plaque formation and stability. Our previous studies have shown that the risk haplotype at the 9p21.3 locus causes defects in VSMC transcriptional program and functions—such as contraction, adhesion, and proliferation. Deletion of the entire locus reverts the risk defect to non-risk status. Here we show that the risk haplotype at 9p21.3 causes impairment in migration and invasion capacity in induced-pluripotent stem cell-derived VSMCs (iPSC-VSMCs). Single-cell RNA sequencing has identified more than 3000 differentially expressed genes (DEGs) between 9p21.3 risk and isogenic knockout VSMCs. Here, we present the generation of a series of tools to perturb some of the top DEGs to assess how these genes are responsible for the risk VSMCs motility defects.

Methods:
Cell culture: VSMC and HEK cell maintenance
Gene expression: RNA extraction, cDNA synthesis, RT-qPCR
Functional Assays: Scratch wound, invasion/migration using IncuCyte S3 live imaging system.
Immunocytochemistry: Staining for genes of interest—LIMCH1, CRABP1
Gain/loss of function studies: cloning of DEGs cDNA and gRNA for silencing into lentiviral vectors, transfection, lentivirus production, infection

Results:
Wound healing assays in iPSC-VSMCs: VSMCs with risk, nonrisk and isogenic knockouts at the 9p21.3 CAD locus were cultured and seeded at maximum confluency. Cells were seeded on gelatin and Matrigel to assay migration and invasion properties, respectively. The VSMC monolayer was scratched using a Woundmaker 96 from Sartorius, and live-cell imaging was used to measure wound closure over a period of 5 days. Risk VSMCs show a reduced invasion capacity when compared with isogenic knockouts.
Wound healing assays in HCA-VSMCs: Heterozygous VSMCs show a reduced invasion capacity when compared to nonrisk.
Gain of function studies on candidate genes LIMCH1 and CRABP1: Through scRNA sequencing we selected *LIMCH1* and *CRABP1* as the most differentially expressed genes in risk VSMCs compared to nonrisk. These two genes were found exclusively in risk cells. We successfully cloned both genes in mammalian expression vectors and tested for proper expression in iPSC-VSMCs.
CRISPR/dCas9 silencing of LIMCH1 and CRABP1: We designed and cloned 4 gRNA sequences for each gene. Lentiviral particles containing the gRNA and dCas9-KRAB enzyme were tested on iPSC-VSMCs.
Analysis of gene expression: RNA from VSMCs treated for overexpression od downregulation of *CRABP1* and *LIMCH1* was collected at multiple time points. RT-qPCR to verify proper silencing/upregulation and to evaluate other gene expression changes in iPSC-VSMCs.

Discussion:
We have successfully used live-cell imaging and scratch assays to measure iPSC-VSMCs ability to perform invasion and migration. These assays have shown that 9p21.3 risk VSMCs are unable to fully close scratch wounds when compared with isogenic knockout VSMCs, suggesting a defect in proper invasion of the extracellular matrix. We have successfully built tools to study the effects of gain/loss of function of top DEGs in 9p21 risk VSMCs and will use them to gain further insight into the invasion and migration defects exhibited by these cells.

Upregulation Of Receptor Interacting Protein Kinase-3 Augments Abdominal Aortic Aneurysms

Jack Bontekoe[1], Ting Zhou[1], Kartik Gupta[1], Huan Yang[1], Amelia Stranz[1], Mitri K Khoury[1], Zulmari Silva-Pedraza[3], Qiwei Wang[1], Bo Liu[1,2]

[1]Div of Vascular Surgery, Dept of Surgery and [2]Dept of Cellular and Regenerative Biology, University of Wisconsin-Madison School of Medicine and Public Health; [3]Dept of Materials Science and Engineering, UW-Madison

Background:
Aortic smooth muscle cell (SMC) depletion is a major pathological feature of abdominal aortic aneurysm (AAA). Our lab has previously reported elevated levels of Receptor Interacting Protein Kinase-3 (RIPK3), a major mediator of necroptosis, in human AAA tissues. Pharmacologic inhibition of RIPK3 or deletion of the *Ripk3* gene prevents aortic SMC death and attenuates aneurysm growth in murine models. In the current study, we tested the hypothesis that manipulation of *Ripk3* gene expression would alter AAA development.

Methods:
We manipulated *Ripk3* gene expression by mutating a conserved putative transcription enhancer site using CRISPR-Cas9-mediated gene editing. AAA was induced in 8-week old male CRISPR mutated (CM) and wild-type (WT) mice by perivascular application of $CaCl_2$ or NaCl (sham). Aortic tissues were harvested on days 4 or 28 post-surgery and analyzed by immunohistochemistry (IHC). Primary aortic SMCs isolated from both groups were stimulated with inflammation-related cytokines and *Ripk3* mRNA was examined by RT-PCR.

Results:
Both CM and WT mice developed AAA in response to $CaCl_2$. Change in aortic diameter was greater in CM mice than WT at 28 days (66.81±4.512 vs 44.87±6.685%, P=0.0108). IHC showed CM aneurysm tissue to exhibit fewer SMCs and a greater number of non-SMC cells in the tunica media, presumably infiltrated immune cells. Furthermore, mutant tissues contained higher levels of RIPK3 positivity than WT aortas. Consistently, CM aortic SMCs expressed more
Ripk3 mRNA than WT SMCs, both with vehicle and following stimulation with IL-1β, IL-25, and IL-33.

Conclusions:
Our data show a positive correlation between *Ripk3* expression and aneurysm size. We are currently analyzing data from experiments aimed to prove the causal relationship between
Ripk3 gene editing, SMC necroptosis, inflammation, and aneurysm growth. This study further illustrates the potential of RIPK3 as a therapeutic target of AAA.

Chronic Mavacamten Treatment Has Opposing Effects on Contractility in Engineered Heart Tissue Models of Severe vs. Mild Hypertrophic Cardiomyopathy

Willem J. de Lange[1], Angeela Gauchan[1], Natalie A. Nelson[1], Emily T. Farrell[1], J. Carter Ralphe[1]
[1]*Department of Pediatrics, University of Wisconsin-Madison*

Background: Many hypertrophic cardiomyopathy (HCM) causing mutations result in myocardial hypercontractility by increasing the number of myosin crossbridges in the disordered relaxed (DRX) state, or by sensitizing the sarcomere to the effects of Ca^{2+}. Mavacamten (Mava) recently became the first FDA-approved treatment of obstructive HCM that directly targets hypercontractility by reducing the number of DRX cross bridges. Mava improves outcomes in patients with obstructive HCM but has not been approved in children or adults without obstructive HCM. The efficacy of chronic Mava treatment at preventing phenotype development in asymptomatic HCM mutation carriers remains largely unexplored. We recently showed that ablation of cardiac myosin binding protein-C (cMyBP-C -/-) in engineered heart tissue (EHT) causes rapid phenotype development in a dish. Initial hypercontractility progresses to hypocontractility with impaired relaxation, mediated by Ca^{2+} mishandling. Here we investigate whether chronic Mava administration prevents phenotype progression.

Methods: cMyBP-C +/+, +/- and -/- EHT were treated with 100nM Mava starting on day 7 of EHT culture. Serial twitch force (TF) measurements were performed weekly for 5 weeks, using the Mantarray platform.

Results: At day 7, prior to Mava treatment, +/- and -/- produced significantly more TF than +/+ EHT (392 ± 9 μN vs. 390 ± 15 μN vs. 199 ± 13 μN). At day 14, Mava treatment reduced TF by 31% ($p < 0.001$) in +/+ EHT, 30% ($p < 0.001$) in +/- EHT and 12% ($p = 0.115$) in -/- EHT. After an additional 4 weeks, chronic Mava treatment reduced TF by 54% ($p < 0.001$) in +/+ EHT, 65% ($p < 0.001$) in +/- EHT but increased TF by 23% ($p = 0.034$) in -/- EHT.

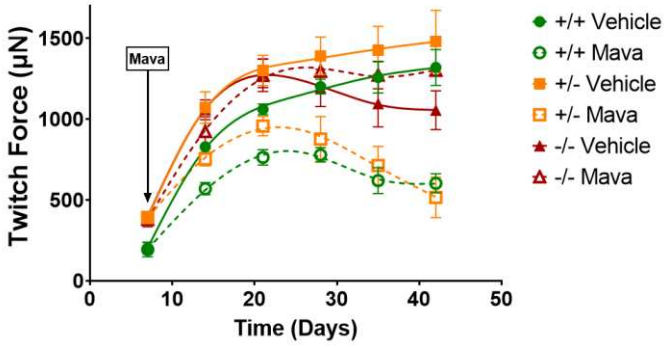

Effect of chronic Mava treatment on twitch force production in +/+, +/- and -/- EHT paced at 1Hz

Discussion: These data show that chronic Mava treatment prevents/slows maladaptive remodeling in -/- EHT, but depresses contractility in +/+ and +/- ECT, suggesting that chronic Mava treatment may be detrimental to patients with mild HCM. Our ongoing studies are assessing the effect of chronic Mava treatment on other EHT models of HCM and on Ca^{2+}-handling.

Noninvasive Assessment of Mechanical Properties Using 4D Flow MRI in a Porcine Model of Aortic Coarctation

[1,4]Stellon, M, [1,5]Gober, L M, [1]Frenkel, A [1,2,3]Roldan-Alzate, A
[1]Department of Radiology, University of Wisconsin-Madison. [2]Department of Mechanical Engineering, University of Wisconsin-Madison. [3]Department of Biomedical Engineering, University of Wisconsin-Madison. [4]Department of Surgery, University of Wisconsin-Madison. [5]Department of Vascular Surgery, University of Wisconsin-Madison

Background

Coarctation of the aorta (COA), a congenital heart disease that results in narrowing of the aorta, triggers pathologic changes throughout the cardiovascular system, including ventricular hypertrophy and flow disturbances. Noninvasive imaging remains a powerful method for studying disease severity, progression and systemic changes without subjecting the patient to ionizing radiation or iatrogenic complications. Our work aims use a porcine model of surgically induced aortic coarctation to study cardiovascular responses to aortic intervention. We expect that by quantitatively defining hemodynamic remodeling, these results will ultimately allow for improved surgical planning and risk stratification.

Methods

A total of 14 piglets were included in this IACUC approved study; 4 sham thoracotomies, 4 coarctation controls and 6 coarctation treatments. Piglets underwent thoracotomy at 2 weeks of age, followed by cardiac MRI, 4D flow MRI and cardiac catheterization imaging at 6, 12 and 20 weeks of life. The coarctation treatment group underwent stent implantation at 6 weeks, with dilations at 12 and 20 weeks. Serial MRI imaging was used to obtain hemodynamic metrics and further computational analysis quantified pulse wave velocity and wall shear stress.

Results

Flow curves between coarctated animals and shams mirror expected patterns. Shams exhibit a higher peak flow with a lower baseline at cycle completion, reflecting greater capacitance and elasticity in a nondiseased aorta. There is no significant difference in net aortic flow distal to the coarctation between sham and control models ($p = 0.097$), however proximally the coarctated animals have lower aortic flow ($p = 0.02$) and higher collateral flow through the internal mammary arteries ($p = 0.0006$). Distal to the coarctation, we would expect collateral vessels to have re-entered the aortic flow stream, validating these findings. All coarcted controls exhibit vortex flow disturbances when pathlines are visually analyzed, whereas none of the sham animals exhibit similar flow vortices.

Discussion

This project uses advanced imaging methods with a focus on 4D Flow MRI, to study hemodynamic changes in the heart and great vessels. Preliminary data validates the coarcted animal as a good physiologic correlate to human aortic coarctation, with expected flow profile changes and compensatory responses. In this study, our goal is to use noninvasive quantitative imaging and derived biomechanics metrics to assess the cardiovascular response to coarctation in a porcine model, with and without intervention. Once fully developed, these metrics can be applied to a variety of aortic conditions.

Sequestration of Alternative Splicing Factors in Cytoplasmic RBM20 Granule Contributes to Aberrant Splicing in RBM20 Cardiomyopathy

Zachery R. Gregorich[1], Yanghai Zhang[1], Yaqin He[1], Eli J. Larson[2], Ying Ge[2,3], Wei Guo[1]
[1]*Department of Animal & Dairy Sciences*
[2]*Department of Chemistry*
[3]*Department of Cell and Regenerative Biology*

Background:
RNA binding motif protein 20 (RBM20) cardiomyopathy is a particularly aggressive form of cardiomyopathy caused by variants in the muscle-specific splicing factor RBM20. Study of patients with RBM20 cardiomyopathy and variant knock-in (KI) animals has revealed that certain variants in RBM20 promote mis-localization and accumulation of the protein in cytoplasmic granules. These cytoplasmic RBM20 granules satisfy the gain-of-function disease mechanism indicated by greater disease severity in RBM20 variant KI versus knockout animal models. Thus, it is currently thought that these granules play an important role in the development of RBM20 cardiomyopathy, yet the molecular mechanism(s) remain unclear. Herein, we utilized in situ proximity labeling in combination with mass spectrometry (MS)-based proteomics to identify the protein components of both cytoplasmic and nuclear RBM20 granules.

Methods:
Constructs for proximity labeling were generated by fusing either WT or S640G variant (analogous to S637G in humans) rat RBM20 to the promiscuous biotin ligase TurboID. TurboID constructs were expressed in H9c2 cells, treated with biotin, and biotinylated proteins were pulled-down using streptavidin and analyzed MS-based proteomics. Protein presence in streptavidin pulldowns was verified by Western blot. Changes in target gene splicing in the hearts of S639G mice were assessed by RT-PCR. Splicing factor co-localization with WT and variant RBM20 was assessed in transfected H9c2 cells using immunocytochemical staining.

Results
Proximity labeling identified 103 and 56 proteins as candidate components of nuclear and cytoplasmic RBM20 granules. Quantitative analysis showed that accumulation of variant RBM20 in the cytoplasm was associated with significant changes in the association of certain proteins with RBM20. In general, there was a decrease in the abundance of proteins implicated in RNA splicing in the environment of variant RBM20, reflecting re-localization of the protein to the cytoplasm. Intriguingly, the alternative splicing factors CELF1 and CELF2 remained among the most abundant proteins in the environment of variant RBM20 and the abundance of MBNL2, another protein involved in alternative splicing, was increased. Western blot confirmed the presence of CELF1 and MBNL2 in streptavidin pulldowns, and ICC demonstrated co-localization with both WT and mutant RBM20 in transfected H9c2 cells. Splicing analysis showed changes in target gene splicing consistent with decreased nuclear MBNL2.

Discussion:
Recently it has been shown that RBM20 variants induce splicing alterations unique from those in knockout animals although the reason is unclear. In this study, we utilized proximity labeling proteomics to identify the components of nuclear and cytoplasmic RBM20 granules. Surprisingly we found that certain splicing factors become sequestered in cytoplasmic RBM20 granules leading to altered splicing of target genes. These findings shed light on a potential mechanism by which pathological variants in RBM20 lead to unique splicing alterations (through trapping of alternative splicing factors in cytoplasmic granules) that may contribute to the development of RBM20 cardiomyopathy.

A Bioanalytical Perspective on AMPK Activation: Phosphorylation, Small Molecule Binding and Isoform Specific Allostery Analyzed with Native and Top-Down MS

Boris Krichel[1,2,3], Hsin-Ju Chan[2], Emily Reasoner[2], Zhan Gao[1], Charlotte Uetrecht[1,3]*, Ying Ge[1,4,5]

[1] *Department of Cell and Regenerative Biology, University of Wisconsin-Madison, Madison, Wisconsin, USA*

[2]*University of Siegen, Siegen, Germany*

[3]*Dynamics of Viral Structures, Center for Structural Systems Biology, Hamburg, Germany*

[4]*Department of Chemistry, University of Wisconsin-Madison, Madison, Wisconsin, USA*

[5] *Human Proteomics Program, School of Medicine and Public Health, University of Wisconsin-Madison, Madison, Wisconsin, USA*

Introduction – 5' adenosine monophosphate-activated protein kinase (AMPK) is the master regulator of cell energy. AMPK dysregulation has been connected to metabolomic disease like obesity and diabetes. AMPK's activation is fine-tuned at different structural stages: tissue specific αβγ-Isoform expression, posttranslational modifications (PTM), heterotrimeric complexation, and allosteric activation. The hallmark of AMPK activation is its ability to directly sense the AMP/ATP ratio in its environment. Moreover, isoform specific AMPK activators have gained increasing interest from the pharmaceutical industry. While the individual stages of AMPK activation have been studied, a detailed analysis of how these stages play together has been elusive. Here, we aim to reveal a comprehensive picture of AMPK activation.

Methods – Three isoforms of the AMPK complex were produced by recombinant expression. Truncated AMPK with increased stability and two full length isoforms, α1β1γ1, was expressed ubiquitously and, α1β2γ1, was expressed particularly in skeletal muscle tissue. To modify AMPK *in vitro*, we used protein phosphatase 2C and a main activating kinase, CaMKK2β. We applied a variety of bottom-up and top-down workflows combined with mass spectrometry analysis using the Bruker MaXis Q-Tof, SolariX FTICR (12 Tesla) and timsToF models. Our workflows combine biochemical and structural characterization with mass spectrometry aiming to reveal the dynamic intramolecular changes occurring during activation of AMPK complex.

Results – First, we focused on analyzing AMPK proteoforms and post-translational modifications. We detected *E. coli* specific (Phospho-)gluconoylation and collected new insights into the N-terminal sequence specificity of this post-translational modification. We located differential auto-phosphorylation between β2 but not β1. We continued with a detailed native MS analysis of heterotrimeric AMPK complex binding to AMP, ADP, ATP and ATγ5P using online native SEC MS. We show that the nucleotide binding sites one, two and three have a high (>10 uM), medium (>1000 uM), and very low (>10000 uM) affinity for AMPK, respectively. We currently are extending this analysis by using other known AMPK interactors to observe binding events from nucleotides, carbohydrates, and small molecule activators at up to 6 different non-covalent binding sites of AMPK. Our analysis reveals in unprecedented detail how AMPK complex is sensing the AMP:ATP ratio in its environment, becomes multiply phosphorylated, and thus changes from an inactive to an active state.

Discussion. Here we present preliminary data of native top-down mass spectrometry platform that reveals a novel, detailed and comprehensive perspective of multistage AMPK activation.

Sphingomyelinase-Induced ROS Production Suppresses Cardiac Performance

Roman Y. Medvedev, Daniel G. P. Turner, Brock W. Thompson, Alexey V. Glukhov
Department of Medicine, Cardiovascular Medicine,
University of Wisconsin-Madison School of Medicine and Public Health,
Madison, Wisconsin 53705, USA

Background: Neutral sphingomyelinase (nSMase) is a hydrolase membrane enzyme that breaks down sphingomyelin into ceramide and phosphocholine. As it was shown in non-cardiomyocyte cells, nSMase can be mechanically activated and participate in the regulation of Ca^{2+} signaling and reactive oxygen species (ROS). However, the role of nSMase in the heart remains unknown.

Methods and results: We applied a high-resolution optical mapping of electrical activity in Langendorff-perfused mouse hearts (n=22). Electrophysiological effects of nSMase activation were determined via perfusion with a bacterial SMase (bSMase, 5 mU/ml). Experimental protocol included a 15-min perfusion with bSMase, followed by reperfusion with a control Tyrode. This resulted in a significant prolongation of action potential duration (APD) and slowing of conduction velocity, accompanied by a decrease in cardiomyocyte excitability (dV/dt), an increase in pacing threshold, and the development of ventricular inexcitability after ~35 min of washout. In isolated cardiomyocytes, 15 min of bSMase incubation reduced Ca^{2+} transient (CaT) amplitude, prolonged CaT duration, and induced a significant rise in spontaneous Ca^{2+} spark activity. Pretreatment with ROS scavenger dithiothreitol (DTT, 2 μM) prevented bSMase-induced conduction slowing, APD prolongation, and decrease in excitability, right-shifting the survival time to 120 mins. DTT also prevented both the reduction of CaT amplitude and the prolongation of CaT duration in isolated cardiomyocytes. Interestingly, pretreatment with DTT did not reduce bSMase-induced augmentation of Ca^{2+} spark activity. In contrast, a selective inhibition of protein kinase A (PKA) with H-89 significantly reduced Ca^{2+} spark frequency after bSMase perfusion. Similar to bSMase, mechanical activation of endogenous nSMase via left ventricular volume overload in *ex vivo* Langendorff-perfused mouse hearts significantly prolonged APD and slowed the conduction velocity. Pretreatment of the hearts with SMase inhibitor GW4869 (5 μM) prevented stretch- induced conduction slowing and APD prolongation.

Conclusions: Our findings indicate that activation of SMase in the heart results in the activation of several pathways possible including ROS and PKA. Overstimulation of these pathways in conditions associated with mechanical overload and inflammation may contribute to the development of arrhythmias and insufficient contractions.

A Missense W792R Mutation in C6 Domain of Cardiac Myosin Binding Protein-C Alters Morphology and Contractility in Neonatal Mouse Myocardium

Jasmine Giles, Ella Harbaugh, Emily Farrell, Richard L. Moss, J. Carter Ralphe

ABSTRACT

Background- Cardiac myosin binding protein-C (cMyBP-C) is a thick filament protein that regulates contractile kinetics. Various mutations within cMyBP-C are a common cause of familial hypertrophic cardiomyopathy. The W792R mutation in the C6 domain of cMyBP-C is known to cause hypertrophic cardiomyopathy (HCM) in humans.

Methods- To examine the impact of mutant W792R on myocardial morphology and contractility, we generated transgenic heterozygote ($W792R^{WR}$) mice expressing both wild-type cMyBP-C and mutant W792R and homozygote ($W792R^{RR}$) mice exclusively expressing mutant MYBPC3. A detailed assessment of morphology, myocardial contractility, and transcriptome response was performed.

Results- No significant differences were found in $W792R^{WW}$ mice compared to $W792R^{WR}$. In contrast, $W792R^{RR}$ mice did not survive past weaning, and had (a) enlarged atria and ventricles, (b) interstitial ventricular fibrosis, (c) a modest decrease in expression of cMyBP-C and increased expression of β-myosin heavy chain, and (d) increased Ca^{2+} sensitivity of force and crossbridge cycling kinetics when compared to $W792R^{WW}$ and $W792R^{WR}$ mice.

Discussion- Collectively, these results suggest that total, but not partial, replacement of cMyBP-C with mutant W792R-cMyBP-C in mice myocardium profoundly alters myocardial contractility and recapitulates phenotypic aspects of severe HCM in human patients.

Functional Impact of Phosphorylation-Site Mutations on PKA Response of Kir2.1

Saba Munawar[1], Corey L. Anderson[1], Louise Reilly[1], Molly Melnick[1], Kyle Brown[2], Ying Ge[2], Lee L. Eckhardt[1].

1. *Cellular and Molecular Arrhythmia Research Program, Division of Cardiovascular Medicine, Department of Medicine, University of Wisconsin-Madison*
2. *Department of Chemistry, University of Wisconsin-Madison*

Background: Kir2.1 channels maintain the cardiac resting membrane potential and assist in phase 3 repolarization. PKA-mediated phosphorylation modulates their function, impacting heart excitability and rhythm. Dysregulated Kir2.1 phosphorylation can lead to various arrhythmias and sudden cardiac death, emphasizing the importance of identifying specific phosphorylation sites and their role in cardiac physiology.

Methods: Eckhardt's lab has identified various novel phosphorylation sites (S13, S14, Y326, T347A, and S313) on Kir2.1. Whole-cell patch clamp experiments of WT-Kir2.1 and listed phosphorylation mutants were performed on stably transfected HEK293 cells using a standard protocol. Cells were perfused with PKA-stimulating cocktail (20μM Forskolin and 10μ IBMX) for 4 minutes. Clampfit 10.7, GraphPad Prism, and Origin 20 were used for Data Analysis.

Result: WT Kir2.1 responds to PKA-cocktail with 2.0 pA/pF increase in maximum outward current and -10 pA/pF change in maximum inward current. The S425A and S14A mutants showed little response to PKA-stimulating cocktail perfusion. The Y326A mutation in Kir2.1 is a loss-of-function mutation, as the residue is thought to be involved in protein folding and channel gating. T347A showed little response to PKA; however, the current is very low at baseline, indicating that this residue may be necessary for PKA-mediated phosphorylation. S13 and S313 mutations showed lower current levels at baseline but responded to PKA stimulation.

Discussion: We identified that S425A and S14A are critical PKA phosphorylation sites on Kir2.1. Further molecular dynamics simulation investigation will provide deeper insight into the conformational changes of Kir2.1 in response to phosphorylation at these sites and the relationship of channel phosphorylation with clinical channel mutation residues.

Identification of Molecular Signatures of Ischemic Cardiomyopathy Using Mass Spectrometry

Melissa R. Pergande[1], Kevin M. Buck[2], Mallory C. Wilson[2], Kalina J. Rossler[1], Morgan M. Mann[1], Scott J. Price[3], Holden T. Rogers[2], Timothy J. Aballo[1], Paul C. Tang[4], Ying Ge[1,2]

[1]Department of Cell and Regenerative Biology, University of Wisconsin-Madison, Madison, WI
[2]Department of Chemistry, University of Wisconsin-Madison, Madison, WI
[3]School of Medicine, University of Wisconsin-Madison, Madison, WI
[4]Department of Cardiovascular Surgery, Mayo Clinic, Rochester, MN

Background: Heart failure is the leading cause of mortality worldwide. Ischemic cardiomyopathy (ICM) is a prominent form of heart failure in which left ventricular (LV) systolic dysfunction reduces blood flow to the heart, resulting in oxygen deprivation and subsequent myocardial hypoxia. Herein, we identified protein changes in cardiac tissues from patients in end-stage ischemic heart failure using mass spectrometry. The results of this study provide insights into the molecular mechanisms underlying heart failure and identifies potential new targets for therapeutic treatment.

Methods: In this study, we utilized bottom-up mass spectrometry to explore the altered proteome in end-stage ischemic heart failure. Human cardiac tissue from failing ICM hearts was collected during left ventricular assist device implantation (n=16). Apex tissue was collected from non-failing donor hearts (n=16). Immediately after dissection, tissues were snap frozen in liquid nitrogen and stored at -80^{o}C until use. Five milligrams of tissue was cryopulverized under liquid nitrogen and homogenized in 5% 4-hexylphenylazosulfonate (Azo) buffer containing phosphatase and protease inhibitors. The concentration of extracted proteins was determined using a Bradford assay. Proteins were reduced, alkylated, and enzymatically digested and analyzed using data independent acquisition PASEF. Peptide data analysis was performed using DIA-NN and relative quantification between conditions was performed using R Studio and DAPAR, DEP R, and IHW R software packages. Pathway analysis of altered proteins was performed to elucidate biological relevance.

Results and Discussion: Herein, we utilized mass spectrometry to profile protein changes in cardiac tissues from patients in end-stage ischemic heart failure. In this study, we identified 7502 protein groups of which 1135 altered proteins were significantly altered between conditions- 747 were increased and 388 were decreased. Pathway analysis of increased proteins includes regulation of complement cascade, FCGR activation, CD22 medicated BCR regulation, extracellular matrix organization, and FCGR3A-mediated phagocytosis. Pathway analysis of decreased proteins includes respiratory electron transport, citric acid cycle, mitochondrial fatty acid beta-oxidation, fatty acid metabolism, and branch-chain amino acid catabolism. Current efforts are focused on identifying metabolomic changes by mass spectrometry analysis, which will allow for an integrated metabolomics and proteomics pathway analysis to aid in determining the functional significance of these molecular perturbations and how they might contribute to heart failure.

Cardiac $Na_V1.5$ Channel Exhibits a p38MAPK-Dependent Modulation

Snizhana Chorna[1], PhD; Marine Sarlandie, PhD[2] Céline Marionneau,[2] PhD; Isabelle Deschênes, PhD[1] and Daniela Ponce-Balbuena, PhD[3]

[1]*Department of Physiology and Cell Biology, The Ohio State University, Columbus Ohio, USA*

[2]*Nantes Université, CNRS, INSERM, l'institut du thorax, F-44000 Nantes, France*

[3]*Division of Cardiovascular Medicine of the Department of Medicine University of Wisconsin-Madison*

Background: Phosphorylation of $Na_V1.5$ channel plays a crucial role in regulating the function and expression of $Na_V1.5$ channels, consequently, modulates I_{Na} and therefore cardiac excitability. Importantly, studies have shown that $Na_V1.5$ channel phosphorylation events may be critical for the genesis of acquired arrhythmias.

The stress-activated p38 Mitogen-Activated Protein Kinases (p38MAPKs) control a wide range of processes. p38MAPKs play a key role in cardiac hypertrophy, myocyte proliferation, and apoptosis. p38MAPKs dysregulations have been linked to numerous diseases, making them a promising pharmacological target for therapeutic use.

The objective of this study was to test whether the human cardiac $Na_V1.5$ channel exhibits modulation by p38MAPK-dependent phosphorylation.

Methods: Our approach includes a combination of biochemical and electrophysiological studies.

Results: Acute activation of p38MAPK decreases I_{Na} density in HEK-293T cells transfected with $Na_V1.5^{WT}$. In patch-clamp experiments, we observed a significant decrease in peak I_{Na} density at -35 mV after acute activation of p38MAPK -139±14 pA/pF compared to control cells -228±30 pA/pF, (p=0.02). Our data showed no changes in voltage-dependence of activation or voltage-dependence of inactivation between groups. However, $Na_V1.5$ channel recovery from inactivation was impaired by p38MAPK activation, we observed a slower recovery from inactivation after activation of p38MAPK compared with control cells, 3.7±0.2 *vs* 4.4±0.2 ms, p=0.02.

On the other hand, acute p38MAPK activation produced no change in $Na_V1.5$ total protein levels even though cell surface biotinylation experiments showed that acute p38MAPK activation reduces $Na_V1.5$ channels' surface expression by ~58%, p<0.05. To identify amino acid residues involved in the p38MAPK phospho-modulation, we mutated putative p38MAPK-dependent serine-proline dipeptide sites S464, S577 and S613 localized in the first intracellular loop of $Na_V1.5$ channel. We observed that the change of $Na_V1.5^{S577}$ and $Na_V1.5^{S613}$ to alanine resulted on loss in the modulation of $Na_v1.5$ channels by p38MAPK, suggesting that p38MAPK phosphorylates $Na_v1.5$ at these two serine residues.

Further, in human iPSC-derived cardiomyocytes, p38MAPK activation reduced the dV/dt_{max} of action potentials, in agreement with an observed reduction in peak I_{Na} density at -10 mV -66±9 *vs* -107±13 pA/pF, respectively, p=0.04. Finally, pre-incubation with p38MAPK inhibitor SB203580 prevented p38MAPK activation-induced effects in HEK-293T and hiPSC-CMs.

Discussion: This work identified a novel p38MAPK-dependent modulation of the cardiac $Na_V1.5$ channel. The study shows that the cardiac $Na_V1.5$ channel is a direct substrate for phosphorylation by p38MAPK protein. Altogether, the results presented provide the first report that p38MAPK signaling may contribute to cardiac $Na_V1.5$ channel regulation and that dysregulation of $Na_V1.5$ channel p38MAPK-dependent modulation, may increase the susceptibility to develop arrhythmias.

AHA Career Development Award 20CDA35320040, DPB, supported this work.

Determining Underlying Mechanisms of Idiopathic VF: A Multi-Disciplinary Approach

Louise Reilly[1], Manasa Kalluri[1], Corey L. Anderson[1], Haibo Ni[2], Di Lang[1], Alexey V. Glukhov[1], Eleonora Grandi[2], and Lee L. Eckhardt[1]

[1] *Cellular and Molecular Research Program, Cardiovascular Research Center, Department of Medicine, University of Wisconsin-Madison, Madison, WI, United States*

[2] *Department of Pharmacology, University of California Davis, Davis, CA, United States*

Background: Idiopathic ventricular fibrillation (IVF) is a clinically challenging disease entity, as phenotypic characteristics are lacking. We studied induced pluripotent stem cell-derived cardiomyocytes (iPS-CMs) from a patient with a PVC-induced IVF (PVC-IVF) to better understand the cellular arrhythmia mechanism.

Methods: iPS-CMs were generated from control (19-9-11) and PVC-induced IVF (PVC-IVF) patient-specific iPSC lines. Calcium-mediated electrophysiological responses were monitored in cell lines via fluorescent single-cell optical mapping using calcium-sensitive dye (Fluo-4 AM) and application of electrical pacing (0.5Hz and 1Hz) before and after administration of 1 x 10-6 mM isoproterenol (ISO)). The experiment was a blind study with respect to cell type, unblinded after data analysis. Statistical analysis was a two-way ANOVA with post hoc Sidak correction for multiple comparisons. Using inversion algorithms optimized for genetic algorithm, we identify differential model parameters driven by PVC-IVF vs. control.

Results: Compared to control, PVC-IVF demonstrates longer calcium transient (CaT) duration, time to peak at baseline and time to 50% recovery. Decay (Tau) and time to 90% recovery was similar between control and PVC-IVF iPS-CMs. We also noted that the PVC-IVF cells demonstrate frequent spontaneous triggered activity and arrhythmic potentials following administration of ISO compared to non-diseased control. Lastly, using our genetic algorithm computational model, we identified significant differences between model parameters for control and PVC-IVF populations. Maximal conductance for I_{to} and L-type Ca^{2+} current was significantly decreased in PVC-IVF compared to control. Additionally, maximum rates for SERCA and Na^{+}/K^{+} ATPase was significantly decreased compared to control.

Discussion: This data demonstrates feasibility and capability of creating patient-specific iPS-CMs and using optical mapping to define experimental distinctions between PVC-IVF and control. Insights from CaT begin to help us characterize arrhythmic substrate and identify molecular players whose activity is altered in this model. This methodology can help uncover the mechanisms for undefined arrhythmias and can be applied to test therapeutics.

Leucine-Rich Repeat-Containing Protein 10 Potentiates L-Type Calcium Current Through Short-N-Terminus and Long-N-Terminus Isoforms of $Ca_V1.2$

Natthaphat Siri-Angkul[1,2,3], Marites T Woon[1,3], Zachery R Gregorich[1,3], Youngsook Lee[4,5], Timothy J Kamp[1,2,3,4,5]
[1]Department of Medicine, University of Wisconsin-Madison
[2]Cellular and Molecular Biology Program, University of Wisconsin-Madison
[3]Cellular and Molecular Arrhythmia Research Program, University of Wisconsin-Madison
[4]Stem Cell and Regenerative Medicine Center, University of Wisconsin-Madison
[5]Department of Cell and Regenerative Biology, University of Wisconsin-Madison

Background: Leucine-rich repeat-containing protein 10 (LRRC10) is a novel regulator of the cardiac L-type calcium channel (LTCC) and several variants of this protein have been linked to dilated cardiomyopathy in humans. We have reported that LRRC10 interacts with the pore-forming ($Ca_V1.2$) subunit of LTCC and potently increases L-type calcium current ($I_{Ca,L}$) in HEK293 cells expressing rabbit $Ca_V1.2$ with long N-terminus encoded by exons 1A and 2. Nevertheless, the effect of LRRC10 on human cardiac LTCCs, which predominantly contain $Ca_V1.2$ with short N-terminus encoded by exons 1 and 2, has never been tested. Moreover, the molecular mechanisms of $I_{Ca,L}$ modulation by LRRC10 remain unknown.

Methods: GST-pulldown assays were performed using purified GST-fusion constructs of the intracellular domains of rabbit $Ca_V1.2$ (N-terminus, transmembrane-domain linkers, and C-terminus) and lysates from HEK293 cells expressing LRRC10 to identify sites of $Ca_V1.2$-LRRC10 interaction. Whole-cell voltage clamp studies were performed to examine $I_{Ca,L}$ in HEK293 cells expressing either human short-N-terminus $Ca_V1.2$ or rabbit long-N-terminus $Ca_V1.2$ and the auxiliary ($\beta_2/\alpha_2\delta$-1) LTCC subunits with or without LRRC10.

Results: LRRC10 was pulled down by the GST-$Ca_V1.2$-N-terminus but not by other GST-$Ca_V1.2$ constructs. LRRC10 increased $I_{Ca,L}$ mediated by human short-N-terminus $Ca_V1.2$ (LRRC10: -165.5 ± 31.2 pA/pF vs. control: -57.4 ± 8.5 pA/pF, $p<0.05$) and rabbit long-N-terminus $Ca_V1.2$ (LRRC10: -81.0 ± 5.3 pA/pF vs. control: -34.1 ± 2.2 pA/pF, $p<0.05$).

Discussion: LRRC10 interacts with the $Ca_V1.2$ N-terminus and potentiates $I_{Ca,L}$ through both short-N-terminus and long-N-terminus $Ca_V1.2$ isoforms, suggesting that the invariant N-terminus segment encoded by exon 2 is the site of $Ca_V1.2$-LRRC10 interaction.

Chronic Angiotensin II Signaling Triggers Sustained PIP_2 Deficits and Altered Sarcolemmal $Ca_V1.2$ Expression and Function in Cardiomyocytes

Taylor Voelker[1], Silvia Garcia del Villar[1], Maartje Westhoff[1], Eamonn Dickson[1], Madeline Nieves Cintrón, Rose Dixon[1].

[1]Dept. of Physiology and Membrane Biology, University of California, Davis, CA.

[2]Dept. of Pharmacology, University of California, Davis, CA.

Background: Contractile dysfunction, hypertrophy, and cell death during heart failure are linked to altered Ca^{2+} handling, and elevated levels of angiotensin II (AngII). This hormone signals through G_q-coupled AT_1 receptors, initiating hydrolysis of phosphatidylinositol 4,5-bisphosphate (PIP_2). Our previous work revealed that acute AngII signaling and PIP_2 depletion destabilizes $Ca_V1.2$ clusters in cardiomyocytes, triggering internalization and acute reduction of whole-cell Ca^{2+} current (I_{Ca}) and contractility. However, the effects of *chronically* elevated AngII on the phospholipid landscape and associated effects on I_{Ca} are under-examined.

Methods: Here, we subjected mice to sustained delivery of AngII to test the impact on phosphoinositides, I_{Ca}, and excitation-contraction coupling using electrophysiology, mass spectrometry, and advanced imaging and biochemistry techniques. We hypothesized that chronic AngII signaling leads to sustained PIP_2 and $Ca_V1.2$ deficits, contributing to the diminished functional output associated with disease development.

Results: Phospholipid mass spectrometry revealed extensive alteration of phosphoinositide species, including a ~44% reduction in PIP_2 and ~37% reduction in cardioprotective PIP_3 in AngII-infused hearts compared to controls. To study the effects of this phospholipid imbalance on $Ca_V1.2$, we examined I_{Ca}, finding similar current density in both groups. However, super-resolution imaging revealed a ~54% reduction in t-tubular $Ca_V1.2$ channel expression and a ~23% reduction in cluster area. Conserved I_{Ca} density despite reduced t-tubular $Ca_V1.2$ would predict that either the channels have relocated to the sarcolemmal crest, or their P_o has increased. We examined crest $Ca_V1.2$ but observed no changes, thus the P_o of the remaining channels must increase to maintain I_{Ca}. Western blots revealed enhanced phosphorylation of $Ca_V1.2$, enhanced phosphorylation of RyR2, and an increase in the catalytic subunit of PKA, suggesting a compensatory sympathetic activation underlying enhanced Ca^{2+} transient amplitude, and conserved I_{Ca}.

Conclusions: These findings support a model wherein chronic elevation of AngII disrupts phosphoinositide and $Ca_V1.2$ levels, elucidating the role of chronic AngII in disease progression.

Effect of mTOR Inhibition on Left Ventricular Function in a Model of LMNA-associated Familial Dilated Cardiomyopathy.

Brittany C Walker, Sindhu Battula, Rachel M Taylor, Allison C Rogers, Timothy A Hacker, Matthew R Wolff

Department of Medicine, Cardiovascular Reserch Center and Model Organisms Core, University of Wisconsin, Madison WI USA

Background: Mutations in the rod-domain of the LMNA (Lamin A/C) gene are associated with a variety of striated muscle diseases in which dilated cardiomyopathy (DCM) is a common finding, with or without associated skeletal myopathies. These forms of inherited or sporadic cardiomyopathies typically result in progressive heart failure, conduction system disease, and malignant ventricular arrhythmias that respond poorly to conventional, FDA-approved medical therapy and result in premature death or the need for cardiac transplantation. Previous studies have suggested that impaired autophagy is involved in the pathogenesis of these disorders, and inhibition of the mTOR pathway can stimulate autophagy and improve cardiac function in murine models. We examined the effects of the mTOR inhibitor rapamycin in a murine double knock-in lmnaN195K/N195K model of LMNA DCM that faithfully recapitulates the human disease.

Methods*: Murine model:* Homozygous *lmna* N195K mice were a gift from Colin Stewart, and faithfully recapitulate the human familial dilated cardiomyopathy phenotype demonstrating cardiac enlargement and dysfunction, conduction system disease and ventricular arrhythmias and premature death at 7 – 8 weeks of age.[5] Wild-type littermates were used as controls, and were treated with vehicle.
Rapamycin Therapy: Rapamyicn (8 mg/kg) or vehicle control was injected once a week starting at 3 weeks of age until sacrifice at 6 weeks for biochemical and histologic studies, or death for survival studies.
Echocardiography: Transthoracic echocardiography (Visual Sonics Vevo 770) was performed to measure left ventricular dimensions and cardiac function using B- and M-mode, and flow velocity in the ascending aorta using pulse-wave Doppler, respectively.

Results: Vehicle-treated mutants demonstrated significantly reduced left ventricular fractional shortening and calculated ejection fraction at six weeks of age compared to wild-type mice. mTor inhibition with rapamycin therapy improved left ventricular systolic function in the mutant mice.

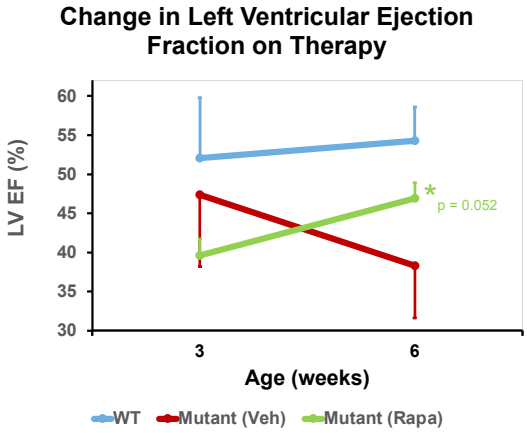

Discussion: Rapamycin improves cardiac function in a disease-relevant murine model of LMNA-associated familial dilated cardiomyopathy
The borderline statistical significance of this finding was limited by the small sample size and an unexpected baseline inbalance in left ventricular function between the two mutant groups. Studies of changes in mTOR and autophagy signaling by Western blotting; nuclear, sarcomeric and cytoskeletal structure by histology; and EM; and survival studies are ongoing.

Mice with Three Major Phosphorylation Sites Ablation on RyR2 Have Normal Adrenergic Response but Increased Susceptibility to Ventricular Arrhythmia

Jingjing Zheng, Holly Dooge, Héctor H. Valdivia, Francisco J. Alvarado
Department of Medicine, Division of Cardiovascular Medicine, and Cardiovascular Research Center, University of Wisconsin-Madison School of Medicine and Public Health, Madison, Wisconsin, USA

Background: Ca^{2+} release through ryanodine receptor 2 (RyR2) is an essential component of cardiac excitation-contraction coupling (ECC), the process that converts action potentials (APs) into mechanical contraction. β-adrenergic signaling is a major regulator of ECC through the phosphorylation of specific targets, including RyR2. However, it's not well understood whether RyR2 phosphorylation is critical for a complete adrenergic response and how RyR2 channel's function is regulated by phosphorylation. To date, three phospho-residues have been well characterized in RyR2: S2030, S2808 and S2814. We created a mouse model with genetic ablation of these three sites (RyR2-S2030A/S2808A/S2814A or triple phospho-mutant [TPM]), to determine the extent to which RyR2 phosphorylation is required for a normal adrenergic response and how the channel's function is changed.

Methods: Mice of 12-20 weeks of age were used for experiments. For in vivo adrenergic stimulation, mice received i.p. injection of 2 mg/kg isoproterenol (Iso). To test arrhythmia susceptibility, mice were given 2 mg/kg epinephrine and 120 mg/kg caffeine by i.p. injection. Adrenergic response in isolated cardiomyocytes was stimulated with 300 nM Iso. Simultaneous action potential/Ca^{2+} transient (AP/CaT) recordings and sarcoplasmic reticulum (SR) Ca^{2+} leak measurements were done in isolated intact cardiomyocytes. Ca^{2+} sparks were recorded in isolated permeabilized myocytes at 50 nM cytosolic free [Ca^{2+}].

Results: TPM mice have normal cardiac structure and function. Upon Iso stimulation, TPM mice have comparable chronotropic and inotropic response to WT, as monitored by ECG and echocardiography. Ca^{2+} transient recorded in isolated myocytes also shows normal response to Iso stimulation. Remarkably, TPM mice are more susceptible to developing bidirectional ventricular tachycardia (BDVT) following arrhythmia challenge (TPM 82% vs WT 0.05%, $n = 22$ per group, $p < 0.01$). To identify the cellular basis of arrhythmia, we first evaluated RyR2-mediated Ca^{2+} leak by three different methods. We measured the susceptibility to diastolic spontaneous Ca^{2+} release (SCR) and delayed afterdepolarization (DAD) by AP/CaT recording after a 20 s pacing train at different frequencies (1 Hz, 2 Hz, 3 Hz). Following 3 Hz pacing train under basal condition, the latency time of the first SCR/DAD event is significantly prolonged in TPM myocytes compared to control (11.09±1.80 s vs 6.50±1.16 s, $p = 0.04$, $n = 21$ in TPM and 19 in WT). Upon Iso stimulation, TPM cells have significantly less frequent SCR/DAD events compared to WT following all pacing trains. These suggest that TPM cells may have less Ca^{2+} leak. We then quantify the total SR Ca^{2+} leak in intact myocytes and sparks-mediated Ca^{2+} leak in permeabilized cells. Total SR Ca^{2+} leak quantification shows comparable Ca^{2+} leak under baseline (WT: 0.140±0.005 $\Delta F/F_0$ $n = 51$ vs TPM: 0.135±0.006 $\Delta F/F_0$ $n = 55$). However, upon Iso stimulation, TPM has significantly less SR Ca^{2+} leak (0.095±0.004 $\Delta F/F_0$, $n = 44$) than WT (0.121±0.007 $\Delta F/F_0$, $n = 50$, $p < 0.01$). Consistently, permeabilized cells have less spark-mediated Ca^{2+} leak than WT (TPM: 48.20±5.90 vs WT: 67.14±4.64 $\Delta F/F_0$*μm^3/100 μm s^{-1}, $n = 42$-44 cells per genotype, $p = 0.01$). The three independent assessments consistently suggest that RyR2-TPM channels are more resistant to Ca^{2+} leak compared to WT RyR2 channels.

Analysis of AP properties from AP/CaT recording shows that TPM myocytes are more susceptible to developing early depolarizations (EADs). Under basal condition, 25% (6/24), 54.17% (13/24) and 76.19% (16/21) of TPM cells developed EADs at 1 Hz, 2 Hz and 3 Hz pacing rates respectively, while only 7.69% (2/26), 11.54% (3/26) and 26.32% (5/19) WT cells have EADs. (WT vs TPM: $p = 0.13$ at 1 HZ; $p = 0.003$ at 2 Hz; $p = 0.005$ at 3 Hz). After Iso stimulation, EAD was induced in 66.67% (8/12) TPM cell while 25% (7/28) WT cells ($p=0.03$).

Discussion: Our data suggests that phosphorylation of the three residues on RyR2 is likely unnecessary for a complete adrenergic response. This, however, does not imply that the sites are not required to regulate RyR2 function. Indeed, the higher incidence of arrhythmia in TPM mice suggests that phosphorylation of the three sites plays a critical role in regulating RyR2 channel function. Our cellular studies consistently show that TPM RyR2 channel has less SR Ca^{2+} leak, suggesting the increased propensity to develop BDVT in TPM mice is not explained by diastolic Ca^{2+} release. The higher incidence of EADs may contribute to the arrhythmia phenotype we observed in TPM mice. Additional experiments will be required to explore this mechanism in detail.

Intricate Roles of Myeloid-derived Thrombospondin-1 in Aortic Aneurysm and Rupture

Ting Zhou[1], Huan Yang[1], Brian Burkel[1], Suzanne Ponik[1], Hong S. Lu[2], Alan Daugherty[2], Bo Liu[1,3]
[1]*Department of Cellular and Regenerative Biology, School of Medicine and Public Health, University of Wisconsin-Madison, Madison, WI 53705, USA*
[3]*Saha Cardiovascular Research Center, Saha Aortic Center, Department of Physiology, University of Kentucky, Lexington, KY 40536, USA*
[2]*Department of Surgery, School of Medicine and Public Health, University of Wisconsin-Madison, Madison, WI 53705, USA*

Background: Abdominal aortic aneurysm (AAA) is the progressive weakening and dilation of the aorta. Aneurysm rupture is the major cause of mortality among AAA patients, but its molecular mechanism is still unclear. We previously reported elevated expression of thrombospondin-1 (TSP1), a matricellular protein, in human and mouse AAA. We also identified Mϕs as the major source of TSP1. In this study, we investigated the role of myeloid-derived TSP1 in AAA and rupture.

Methods and Results: Male myeloid-specific TSP1 deficient mice (*Thbs1*$^{\Delta M\phi}$) and wildtype littermates (*Thbs1*^{wt}) were challenged with angiotensin II (Ang II) coupled with hypercholesterolemia. Sixty-one percent of *Thbs1*$^{\Delta M\phi}$ died from AAA rupture, an incidence that was 2.6 times higher than *Thbs1*^{wt} (n=23 for *Thbs1*^{wt}, n=30 for *Thbs1*$^{\Delta M\phi}$). Intriguingly, *Thbs1*$^{\Delta M\phi}$ that survived to the end of 28-day Ang II infusion had less aortic dilation than *Thbs1*^{wt}. Majority of the rupture occurred between 7 to 14 days of Ang II infusion. Ultrasound imaging at early time points (baseline, 3 or 7 days after AAA induction) showed no difference in the aortic diameters between genotypes. To understand the molecular mechanisms underlying the rupture-prone phenotype of *Thbs1*$^{\Delta M\phi}$, we conducted single-cell RNA sequencing on the aortic tissues 7 days after AAA induction. *Thbs1*$^{\Delta M\phi}$ showed increased percentages of smooth muscle cells (SMCs), and decreased Mϕs and fibroblasts. Six functional SMC subclusters were identified, which were contractile, fibroblast-like, proliferative, macrophage-like, hemoglobin positive, and intermediate SMCs. *Thbs1*$^{\Delta M\phi}$ specifically increased the intermediate SMCs, all the other subclusters were decreased. Pathway analysis revealed an extended reduction of extracellular matrix-related genes. Histological analysis confirmed the predicted matrix weakening caused by the myeloid-specific TSP1 deficiency.

Discussion: Myeloid TSP1 is critical for Mϕ infiltration, which fuels aneurysm growth. However, Mϕs, likely through signaling to SMCs and fribroblasts via TSP1, may also contribute to the vascular remodeling at least in the Ang II-induced aortopathy. Therefore, *Thbs1*$^{\Delta M\phi}$ provides a unique model to investigate the complex interplays between Mϕs and vascular cells in AAA and rupture.